Development of a Gridded Energy Analyzer for Measurement of the Mochi Experiment Ion Energy Distribution

Morgan Quinley

A thesis
submitted in partial fulfillment of the
requirements for the degree of

Master of Science

University of Washington

2015

Reading Committee:
Dr. Setthivoine You, Chair
Dr. Uri Shumlak

Program Authorized to Offer Degree:
Aeronautics & Astronautics

University of Washington

Abstract

Development of a Gridded Energy Analyzer for Measurement of the Mochi Experiment Ion Energy Distribution

Morgan Quinley

Chair of the Supervisory Committee:
Assistant Professor Dr. Setthivoine You
Department of Aeronautics & Astronautics

A new experiment at the University of Washington called Mochi is intended to simulate astrophysical jets in the laboratory and investigate their stability, with particular interest in conservation of canonical helicity. As a new experiment, Mochi's plasma parameters are relatively unknown. This thesis describes the development of a gridded energy analyzer (GEA), the ultimate goal of which is to provide initial measurements of Mochi's ion energy distribution. The concept of the Mochi.GEA is to start with the simplest possible design and make necessary improvements based on observed performance. The initial design suffered from a space charge limitation issue, which was mitigated using a pinhole aperture. Secondary electron emission was also identified as a major issue and addressed with a secondary electron suppressor. The analyzer has successfully measured the electron energy distribution but not yet successfully measured the ion energy distribution. However, the Mochi.GEA design is easily modifiable, and further development may arrive at a working design.

TABLE OF CONTENTS

LIST OF FIGURES

ACKNOWLEDGEMENTS

I would like to thank Dr. Setthivoine You, Jens von der Linden, Evan Carroll, and the rest of Mochi Lab for their support during this work. Upon entering this program I knew nothing about electronics or scientific computing. By the end I had built a TTL-to-optical transmitter array, debugged high-pulsed-power supplies, written complex Python scripts, and developed a gridded energy analyzer. None of this would have been possible without their expertise and willingness to help.

I would also like to thank Dr. Uri Shumlak for patiently teaching me the fundamentals of plasma physics and reviewing this thesis. Finally, I'd like to thank my graduate advisors Ed Connery and Wanda Frederick for their advice and assistance on innumerable topics throughout the past two years.

1 INTRODUCTION

Mochi is a new experiment at the University of Washington intended to simulate astrophysical jets in a laboratory. These naturally occurring plasma jets are among the largest structures in the Universe and are remarkably stable, whereas columnar plasmas created in a laboratory tend to rapidly kink and break up. The primary goal of Mochi is to determine the degree to which the conservation of canonical helicity (the vector sum of fluid vorticity and magnetic field helicity) contributes to this observed stability. In order to do this, Mochi employs a large (1.4m diameter), spherical vacuum chamber with a pair of planar plasma guns. The first gun (Mochi.SpheromakGun) has two concentric electrodes made up of a central copper disk and a copper annulus linked by a dipole background magnetic field. The arrangement is designed to replicate the geometry of an accretion disk around a central object that serves to launch astrophysical jets. The radial electric field from the voltage potential drop between the electrodes combines with the poloidal magnetic field to reproduce the azimuthal plasma rotation in an accretion disk. The second gun (Mochi.LabJet) has an additional concentric annular electrode to produce a shaped radial electric field and therefore shear azimuthal rotation. Combined with azimuthally symmetric gas sources, the setup provides more realistic boundary conditions for magnetic plasma jet shear flow stabilization and collimation. During an experimental shot, gas is injected between the electrodes of the gun and broken down into plasma along the arched field lines of a background magnetic field. The current driven through this arched plasma pinches the plasma into a tight jet geometry extending from the gun.

This experiment will use vector tomography of ion Doppler spectroscopy and high-density magnetic probe arrays to measure the canonical helicity components of the jet. Multichord interferometry will also be used to measure the density of the plasma jet. These diagnostics are not yet operational, and as a new experiment Mochi's parameters are relatively unknown. For this reason, there is interest in implementing basic diagnostics that can provide important information about the Mochi plasma. High-voltage probes are used to measure gun voltage, and current monitors are used to measure the gun current and bias field discharge. A high-speed camera is used to capture images of the plasma, which provides important information about the

geometry of the plasma. This thesis details the design and implementation of another diagnostic: the gridded energy analyzer.

Plasma energy analyzers, or retarding-field analyzers (RFAs), are electrostatic diagnostic devices used to measure the energy distribution of plasma particles. The most common type is the gridded energy analyzer (GEA), which has been used by many experiments to measure the ion energy distribution of plasmas for many years. The GEA is a popular plasma diagnostic because it can be very simple to design and build and is one of few devices that measures the microscopic properties of a plasma. Whereas most plasma diagnostics are sensitive to macroscopic quantities like temperature, pressure, density and magnetic field, a retarding-field analyzer is sensitive to the energy of the individual particles that enter it. This allows the distribution of particle energies to be constructed. Once this distribution is known, taking its various moments can retrieve the macroscopic detail of the plasma. Furthermore, knowledge of the shape of the energy distribution can be used to validate or invalidate critical assumptions commonly made in plasma physics experiments. The use of magnetohydrodynamic (MHD) theory to describe plasma phenomena requires that the particle energy distribution be closely approximated by the Maxwell-Boltzmann distribution. Also, the relative shapes of the ion and electron energy distributions can determine whether the plasma is in thermal equilibrium.

Although the GEA is a common plasma diagnostic, there are a few important issues associated with its use. Proper interpretation of RFA signals requires careful consideration of sheath effects and collective behavior within the device. Furthermore, as electrostatic probes, retarding-field analyzers sometimes suffer from significant electrical noise, which can make the signal impossible to recover. Also, the measurement is local, which requires the probe to be located at the point of interest within the experiment. This is often limited by practical considerations like perturbative effects and the maximum heat flux that the probe can withstand. Typically the particle energy distribution must be constructed over many shots, which introduces experiment repeatability into the measurement. These issues can be overcome using fast electronics and reciprocating probe designs [1], but these can be very complicated and are only applicable if the plasma is sufficiently long-lived. However, in spite of these issues the simplicity of the retarding-

field analyzer makes it one of the most feasible choices if the ion energy distribution is of interest.

The motivation for the development of this gridded energy analyzer is multi-faceted. The major impetus is to provide fundamental information about the Mochi plasma, including the ion energy distribution and temperature. The rate at which the plasma expands or propagates across the Mochi vacuum chamber is also easily measureable. This information will be compared to that of similar experiments in order to ensure the Mochi plasma is behaving as expected, and may be used to corroborate future diagnostics. This GEA may also provide useful physics results of its own by identifying non-Maxwellian particle energy distributions. A similar experiment at Caltech [2] has observed macroscopic instabilities related to magnetic reconnection events occurring in the kinetic (microscopic) regime. Similar behavior in the Mochi plasma may be elucidated by the GEA results. However, the scope of this thesis is not to make physics observations, but to describe the design, operation and issues of Mochi gridded energy analyzer.

2 GRIDDED ENERGY ANALYZER THEORY & OPERATION

Gridded energy analyzers operate on the principle of selective electrostatic repulsion of electrons and ions. Figure 1 shows a diagram of a gridded energy analyzer set up to measure the ion distribution. Plasma particles enter the device and encounter the electron repeller grid, which is held at a potential, ϕ_{e-r}, sufficiently negative to repel almost all of the electrons. The ions pass through this grid and encounter the ion repeller grid at a positive potential, ϕ_{i-r}. This grid repels any ions with kinetic energy less than $E_{min} = q_i\phi_{i-r}$, where q_i is the ion charge. This truncates the lower-energy portion of the ion energy distribution, $g(E)$, as shown. The remaining ions then strike the collector and their current, I_c, is measured.

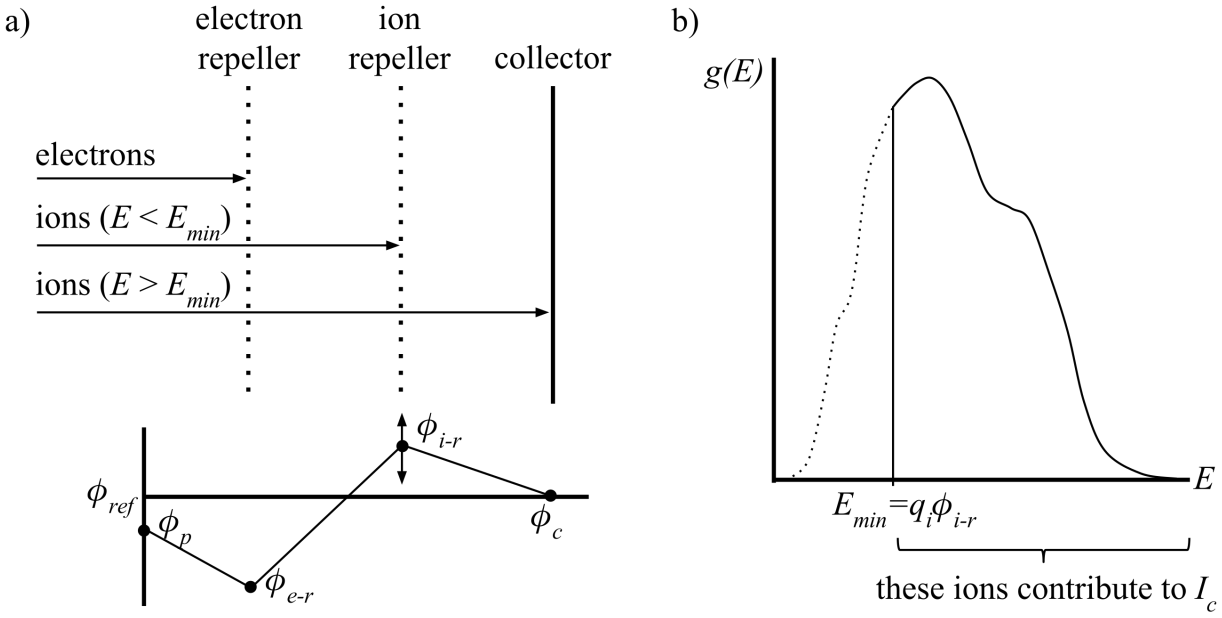

Figure 1. A diagram of a gridded energy analyzer set up to measure the ion distribution is shown in a). Plasma particles are repelled by the electron and ion repeller grids. The ion repeller potential is adjusted to control the number of transmitted ions, which strike the collector and contribute to the measured collector current. The lower-energy portion of the ion energy distribution is thus truncated at the minimum energy, as shown in b).

GEA operation involves increasing the ion-repeller potential from 0V and recording I_c until no current is measured (i.e., all of the ions are repelled). This allows the collector current as a function of minimum energy, $I_c(E_{min})$, to be experimentally determined. The collector current is equal to the integral of the current density over the collector area, A_c. The current density is equal to the product of the ion charge, q_i, and the ion flux, $\vec{\Phi}_i$, assuming that only ions contribute to the current.

$$I_c = \int_{A_c} q_i \vec{\Phi}_i \cdot d\vec{A} \tag{1}$$

The ion flux is the first moment of the ion velocity distribution, $f(\vec{v}_i, \vec{x}_i)$, evaluated from the minimum velocity associated with E_{min} to infinity. This is a six-dimensional distribution in velocity-position space. However, the GEA resolution is not sufficient to measure all six dimensions. The GEA is a local diagnostic, so the spatial variation of the distribution can only be determined by moving the probe or using multiple probes. For a given probe location, the spatial resolution in the plane of the collector is limited to the collector area. Thus, it must be assumed that the distribution is uniform over the entire collector area: $f(\vec{v}_i, \vec{x}_i) \rightarrow f(\vec{v}_i)$.

As implied in the collector Equation (1) above, the GEA is only able to resolve particle motion along the axis normal to the collector (in the direction of $d\vec{A}$, here defined as z). Furthermore, the device only measures particles with positive component of velocity toward the collector. Any particle motion not in this direction, as well as its associated energy, is not measured: $f(\vec{v}_i) \rightarrow f(v_{i,+z})$. If the GEA measures particles in a very small solid angle, it can be reasonably assumed that this is the dominant component of $f(\vec{v}_i)$. For the remainder of this analysis the "+z" subscript is dropped and the one-dimensional velocity and energy distributions, $f(v_i)$ and $g(E)$, are used. Under these restrictions, I_c becomes:

$$I_c\left(v_{\min}\right) = q_i \Phi_i A_C = q_i A_C \int_{v_{\min}}^{\infty} v_i f\left(v_i\right) dv_i \tag{2}$$

A simple change of variables can be used to convert from velocity to energy in this integral. The kinetic energy of each particle obeys the relation

$$E = \frac{1}{2} m_i v_i^2 \rightarrow v_i = \sqrt{\frac{2E}{m_i}}, \tag{3}$$

where m_i is the ion mass. Furthermore, the quantity $f(v_i)dv_i$ corresponds to the number of particles in a band of the distribution $f(v_i)$ of width dv_i centered at v_i. This must be equal to the number of particles in a band of the corresponding energy distribution, $g(E)$, of width and location determined using Equation (3). Thus, by definition, $f(v_i)dv_i = g(E)dE$. Using this definition and Equation (3), I_c becomes:

$$I_c\left(E_{\min}\right) = q_i A_c \int_{E_{\min}}^{\infty} \sqrt{\frac{2E}{m_i}} g\left(E\right) dE \tag{4}$$

Equation (4) relates the measured collector current to the ion energy distribution. The distribution can be retrieved from this expression by taking its derivative with respect to E_{min}. Reversing the bounds on the integral and using the statement of the fundamental theorem of calculus, $F(x) = \int_a^x f(t)dt \rightarrow dF(x)/dx = f(x)$, the derivative is:

$$\frac{dI_c\left(E_{\min}\right)}{dE_{\min}} = -q_i A_c \sqrt{\frac{2E_{\min}}{m_i}} g\left(E_{\min}\right) \tag{5}$$

Rearranging this expression and recognizing that the distribution of repeller energies, $g(E_{min})$, is equal to the distribution of particle energies, $g(E)$, the ion energy distribution is found to be:

$$g(E) = -\frac{1}{q_i A_c}\sqrt{\frac{m_i}{2E}}\frac{dI_c(E)}{dE} \tag{6}$$

The units of $g(E)$ are particles per unit volume per unit energy, commonly expressed as particles/m^{3}eV. This requires an additional factor of $1/c$ or $1/\sqrt{e}$ if the units of E are eV and the units of m_i are eV/c^2 or kg, respectively, where c is the speed of light and e is the electron charge.

In order to use this method to obtain the ion energy distribution from experimental data, a few practical matters must be considered. What is actually measured is a potential trace (e.g. via oscilloscope), $\phi_m(t)$, not the collector current itself. First, the time-dependence of the measurement must be dealt with during analysis[1], and the simplest practice is to use the peak value. Alternatively, the signal can be integrated in time and the total collected charge can be used. Strictly speaking, this method changes the units of Equation (6) so that the factor $\sqrt{m_i/2E}$ must be replaced with a characteristic length.

Second, the measured potential can be converted to collector current by convolving the signal with the inverse of the frequency-dependent impedance of the measurement line. This impedance can be determined either by estimation based on the geometry of the probe, or by calibration. However, this conversion serves only to scale the amplitude of the measured energy distribution and does not affect its shape or location, which are of far greater importance. Thus, this procedure can be avoided if the scale and units of $g(E)$ are reported as arbitrary:

$$g(E) \sim -\frac{1}{\sqrt{E}}\frac{dI_c(E)}{dE} \quad \text{[arbitrary units]} \tag{7}$$

The ion-repeller potential is typically held fixed during a shot and increased over many successive shots, which means that the determined $I_c(E_{min})$ includes any shot-to-shot variability.

[1] *This does not apply to GEAs with electronics fast enough to sweep* ϕ_{i-r} during a shot.

This requires several shots to be taken at each ion-repeller potential, and their average I_c to be used. GEAs with sufficiently fast electronics compared to the plasma lifetime may be able to sweep the repeller potential and measure $I_c(E_{min})$ during a single shot, but shot-to-shot variability should still be considered [1].

Finally, Figure 1 indicates that particles enter the device at some potential, ϕ_p, associated with the plasma. If the device is not referenced to this potential (i.e. $\phi_{ref} \neq \phi_p$), then the measurement includes some portion of it. In practice this is difficult to achieve, because any conductor used to measure the plasma potential actually measures the floating potential. Therefore, it is common to reference the device to a more convenient potential, such as that of the vacuum chamber. This also means that if particles enter with a potential less than the electron-repeller potential or greater than the ion-repeller potential, they will not be repelled.

3 MOCHI.GEA DESIGN

3.1 DESIGN CONSTRAINTS & CRITERIA

The typical design of a gridded energy analyzer involves consideration of collective effects. Plasma that enters the device will tend to shield the applied potential of the repeller grids, rendering them ineffective, over distances on the order of a few Debye lengths. This requires the grid hole size to be on the order of the Debye length and the separation between the grids to be on the order of ~4 Debye lengths. This requirement can be very difficult to meet in practice, as the Debye length can be quite small. A common solution to this issue is to use a pinhole aperture and/or a low-transparency grid to reduce the density of the plasma that enters the device, thereby increasing its Debye length to a feasible level. However, this also reduces the amplitude of the ion current, possibly to a level below that of the electrostatic noise. [4]

Since Mochi is a new experiment its plasma parameters are relatively unknown, making it difficult to base the design of the GEA on the Debye length. In order to avoid the complications that this imposes, the concept of the Mochi.GEA is to begin with the simplest possible design and modify it in response to observed issues. Furthermore, the Mochi vacuum chamber has a

large radius (~ 70cm) compared to the radius of the plasma jet (~ 3.5cm), so the majority of the chamber should be in good vacuum (base pressure < $2x10^{-6}$ torr), filled with very diffuse (large Debye length) plasma or even particles in the single-particle regime. It is possible that a GEA designed without regard for the Debye length could successfully operate in this region.

The typical GEA signal amplitude is quite small, on the order of microamps [1]. This often requires amplification. In order to avoid this, the collector area should be made as large as possible to collect the largest signal. This comes at the cost of spatial resolution in the plane of the collector. However, without the aid of a complicated translation system, the spatial resolution of the GEA is limited by the location of vacuum chamber ports, not the collector size.

There are two additional design criteria for the Mochi.GEA. The Mochi vacuum chamber has many ports on which the GEA could mount, but most of them are allocated for tomographic optical collectors. The majority of remaining ports are 2.75in CF vacuum flanges, so the Mochi.GEA is designed to mount to this vacuum interface. It is also desired that the probe be small enough to fit through this port, so that the chamber door does not need to be opened in order to install or remove it. Furthermore, in order access the large volume and entire range of plasma parameters, the depth of the probe must be adjustable and able to cover the radius of the chamber.

3.2 Electronics Design

The Mochi.GEA circuit diagram is shown in Figure 2. The lead wires to the grids and collector run through the inside of the probe arm and are terminated as grounded BNC connectors on an electronics enclosure. Coaxial cables connect these to an oscilloscope and two power supplies: one biased positive and one negative with respect to common. The scope and supplies are powered from wall power via an isolation transformer, to which they are plugged in using cheater plugs. This ensures that the oscilloscope and supplies are grounded only through the BNC cables and GEA electronics enclosure to the experiment “Spider Point” (common ground connection point), avoiding ground loops. This also means that the reference potential for the GEA (see Figure 1) is the experiment ground. Since Mochi is a pulsed, high-power experiment, this ground likely fluctuates during a shot. For this reason, the fourth BNC connection on the

electronics enclosure is used with channel A of the oscilloscope to measure the floating reference potential for subtraction from the GEA signal. This circuit design is the most successful of many tested designs, as discussed in section 4.1.

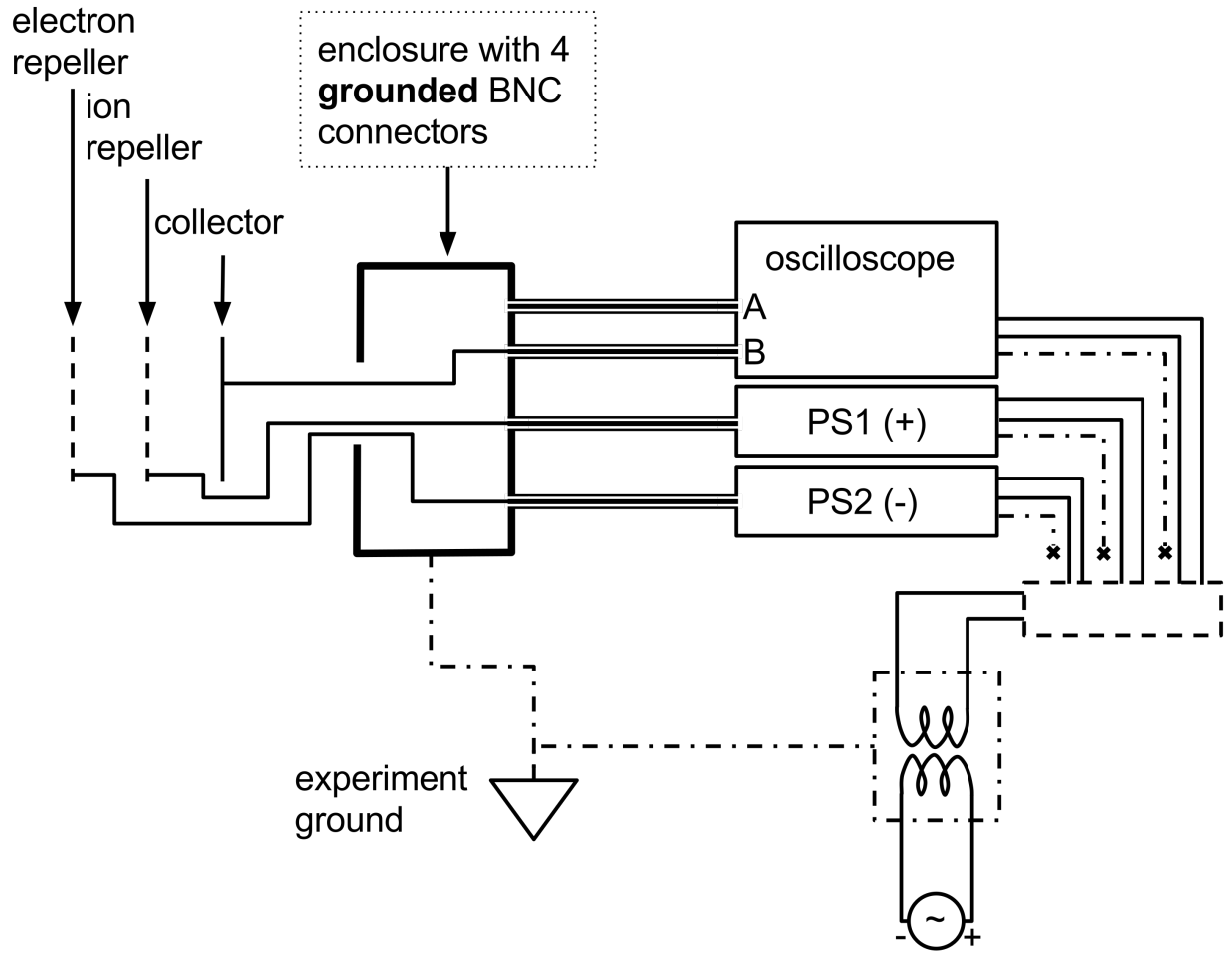

Figure 2. Mochi.GEA circuit diagram.

3.3 GEA Mechanical Design Concept

The Mochi.GEA consists of ion and electron repeller grids, a collector, and several other components. The grids and collector of the GEA must be electrically isolated from each other and shielded from the rest of the plasma. Both of these functions are performed by ceramic insulation rings, one for each grid and one for the collector, which make the intragrid distance 6.35mm (0.25in). Each grid and the collector are also compressed against an electrical contact ring, which provides electrical access. A pinhole aperture and spacer ring are attached to the

front and back of the probe head and serve to limit the plasma flux and guide the lead wires, respectively. This stack of components comprises the probe head of the GEA.

The probe head is exposed to vacuum but the grids/collector must be powered/measured from the air side of the chamber. This is achieved on the Mochi.GEA using a custom electrical feedthrough made from two modified 1⅓in CF vacuum flanges. The GEA probe head is mounted to one side of this vacuum seal using three #4 screws and the other side is welded to the probe arm. This probe arm extends back through an O-ring seal mounted to a 2.75in CF flange on the vacuum chamber. Wires are passed from the vacuum side through the feedthrough and probe arm to an electronics enclosure mounted at the end of the probe arm, where they are terminated as coaxial BNC connectors.

Exploded views and photographs of the Mochi.GEA assembly are shown in Figure 3 and Figure 4. The probe head is cylindrical with the same outer diameter as the 1⅓in CF vacuum flanges making up the vacuum seal. This maximizes the interior diameter available for collector area, while allowing the entire probe to be inserted through the port to which it is mounted. The current design includes an aperture, electron repeller grid, ion repeller grid, secondary electron suppressor (not shown) and collector. The modular design allows the probe head to be easily modified by inserting or removing components from the stack. For example, the photograph shows that an aluminum disc, or gate, has been installed on the front of the probe head. This gate (at least partially) blocks plasma from entering the device, and can be opened and closed by rotating the probe.

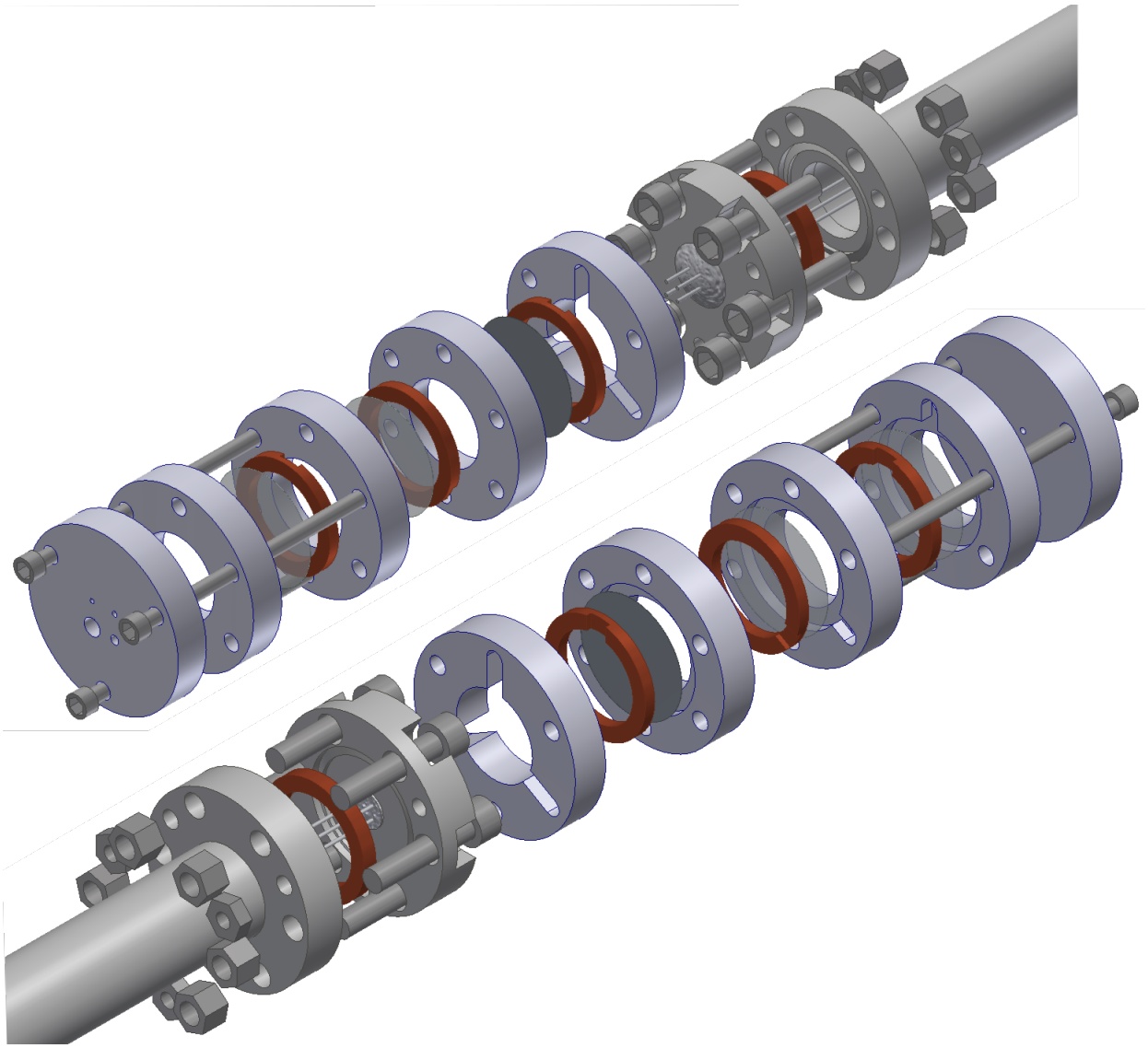

Figure 3. An exploded view of the Mochi.GEA, including two grids and an aperture.

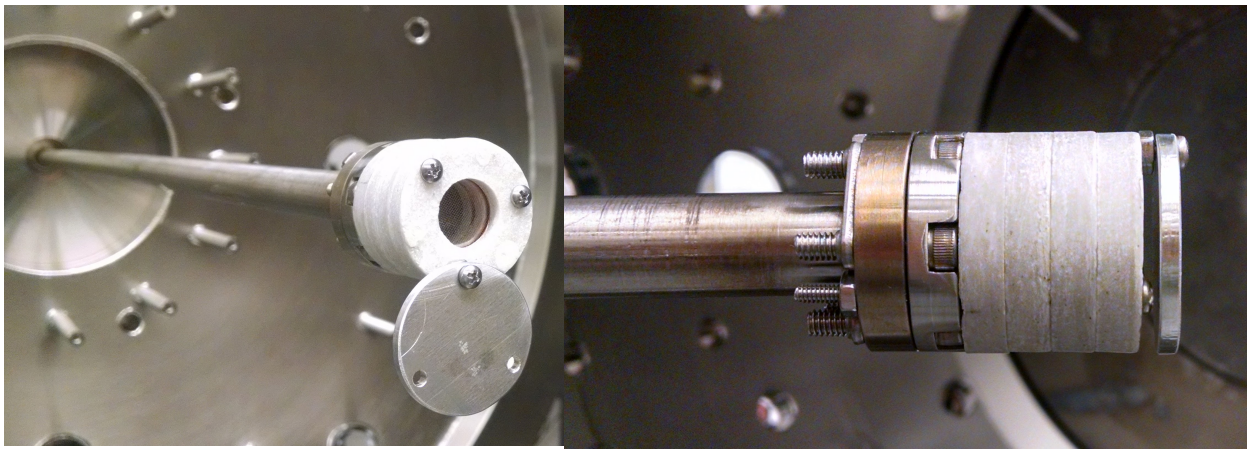

Figure 4. Photographs of the Mochi.GEA installed on the vacuum chamber. The photograph on the left shows the interior of the GEA, including the grids, electrical contacts, and collector. This design iteration includes only two grids.

Each of the components of the Mochi.GEA is described in more detail in the following sections.

3.4 Probe Head

3.4.1 *Grids*

The grids of a GEA will necessarily intercept some portion of the incident particle flux, effectively decreasing the collector area. For this reason, it was important to use a grid material with the highest possible transparency that is commercially available. The grids of the Mochi.GEA are made from an off-the-shelf wire mesh sheet, purchased from TWP Inc. The wire mesh is made of type 316 stainless steel and has a hole size of 0.48mm, thickness of 0.06096mm, and transparency of 88%.

Type 316 stainless steel is non-magnetic and has a moderate coefficient of secondary electron emission [3], both of which are important for this application. However, it has a relatively high resistivity compared to other commonly used grid materials, about 10 times greater than that of nickel and 40 times greater than that of most copper alloys. The geometry of a grid also leads to a much higher resistance than a solid sheet. Since the grids will intercept some of the flux they must draw a current during a shot in order to sustain their applied potential. If the resistance of a grid and the current it draws combine to exceed the maximum power output of its supply, the potential of the grid will vary during the shot, confounding the measurement.

The wire mesh is thin enough to be cut by a pair of scissors or a razor blade, but also so thin that they are difficult to handle without severely distorting them. The grids were made by clamping the mesh between a metal plate and a metal cylinder slightly less than the desired grid diameter of 21mm (see section 3.4.3). The grids were then made by cutting around the cylinder with an x-acto knife. This method allowed grids to be made with distortion only around the edge, which will not be visible to the plasma.

3.4.2 *Collector*

The Mochi.GEA collector is made from a tantalum foil, left over from use in the Mochi.FIG (Fast Ion Gauge). Tantalum was used in the FIG for its moderately low resistivity and high density, which is important for collection of high-energy ions. This foil is about the same thickness as the grids (0.0635mm), and is made to the same diameter (21mm). This foil was stiff enough to be cut out using a pair of scissors.

3.4.3 *Electrical Contacts*

The grids and collector require lead wires that run back to the electrical feedthrough, but these components do not readily accept solder. Furthermore, a wire connected to one point of the high-transparency grid may not provide an adequate electrical connection. These issues are solved by the electrical contacts: a copper ring to which a short length of wire has been soldered. These contacts are compressed against the grids and collector when the probe head stack is assembled, ensuring an acceptable electrical connection. The wire is soldered into a shallow notch filed into the copper ring, and then the solder is trimmed in order to ensure that the wire and solder to not exceed the height of the copper ring. This allows the electrical contacts to be compressed evenly and prevents gaps between the insulation rings. The copper rings are filed down to size from used gaskets for 1⅓in CF vacuum flanges and the wire is 32 gauge magnet wire.

3.4.4 *Insulation Rings*

The insulation rings must be made out of a machinable, electrically insulative material that can withstand a high-vacuum environment. The material chosen for this purpose is a machinable ceramic called Mykroy/Mycalex®, purchased in the form of a 6.35mm (0.25in) thick sheet. This

material has a dielectric strength of 20.9kV/mm, is nonporous, and does not outgas. The insulation rings were carefully machined from the sheet using an end mill, and are thus 6.35mm thick.

In addition to insulating and shielding the grids, the insulation rings establish some of the important geometry and dimensions of the Mochi.GEA. When stacked together, the thickness of the rings gives rise to an intragrid distance of 6.35mm. The rings have an outer diameter of 33.8mm (1.331in), which is the same as that of the vacuum seal and defines the outer diameter of the probe head. Six evenly spaced holes pass through the rings near the outer edge. These holes are large enough to accept a #4 screw for mounting to the vacuum seal. Within this hole pattern is a shelf in which the grid/collector and its electrical contact ring will sit. The collector size is a function of all of these dimensions: collector radius = outer radius – mounting screw hole diameter – shelf width – appropriate wall thicknesses. This spatial constraint and consideration of machinability resulted in a collector area of 198mm^2 (0.307in^2), corresponding to the diameter of a 5/8in end mill bit.

Three of the six holes near the edge of the insulation rings are used for mounting screws and the other three are used to transmit lead wires to electrical contacts, if necessary. The space between the shelf and one of the six holes is milled out to form a channel for the wire to pass through. The wire is then passed through the corresponding hole of the other insulation rings between it and the vacuum seal. An additional ceramic piece, the spacer ring, sits between the collector and the vacuum seal and provides some room for lead wire management.

Since the lead wires to the grids must pass through all of the preceding insulation rings, the stack of insulation rings is essentially wired together. Also, it was desirable to make the insulation rings for each grid non-unique. But if an aperture is not used the holes in the forward-most insulation ring allow the plasma access to the lead wires and the back of the collector. This can be remedied by filling in the three unused holes with high-vacuum compatible epoxy (Torr Seal®), as can be seen on the left in Figure 4. These oversights somewhat limit the modularity of the Mochi.GEA. If components are added to or removed from the probe head in the future, the device may need to be rewired and the insulation rings modified or replaced.

The engineering drawings of these insulation rings can be found in Appendix A.

3.4.5 *Aperture*

In order to achieve the maximum possible collector area, the initial design of the GEA did not include an aperture. In response to several issues (see section 4.2) an aperture was later installed on the device, as shown in Figure 5. The aperture was machined out of the same ceramic sheet and mounted to the probe head in the same way as the other components. It was made with 4 holes of various sizes, with the idea that these could be selectively blocked to control the open area. Prior to installation all but the smallest hole (diameter of 0.91mm) were blocked using a common vacuum cement (Torr Seal®). The diameter of the pinhole is that of a #64 drill bit (0.9144mm), which was used because smaller drill bits broke when tried. This aperture corresponds to about a 26x reduction in solid angle and a 17x reduction in open area.

Figure 5. A photograph of the Mochi.GEA with the pinhole aperture and gate installed. The other three holes filled in with Torr Seal® are visible as well.

An engineering drawing of aperture can be found in Appendix A.

3.5 Vacuum Components

The vacuum seal disc is intended to provide a vacuum-tight electrical feedthrough for the GEA wires. This was achieved by using the vacuum seal of two blank 1⅓in CF vacuum flanges and modifying them to accept wires, as shown in Figure 6. One flange has a hole bored through its center with a countersink one the side opposite the seal. This countersink butt-welded to a stainless steel tube, creating the probe arm. The second flange also has a hole bored through its center, which is used for the electrical feedthrough. A small Teflon disc with four small holes in it is pressed into hole in the flange. Four wires are inserted through the disc, which serves to electrically isolate them, as can be seen in the image on the left. The vacuum side of the flange is sealed with Torr Seal® so that no Teflon is exposed to vacuum.

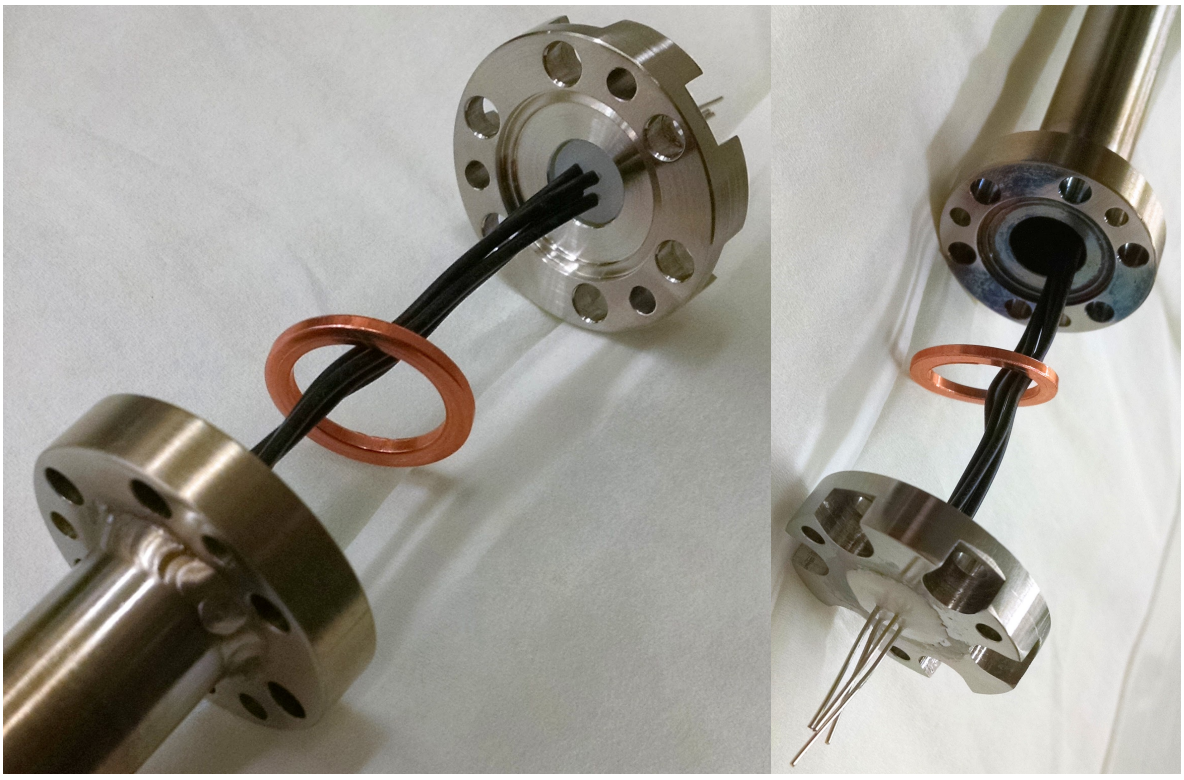

Figure 6. Vacuum seal subassembly.

On the air side the wires are inserted through a copper gasket and run down the probe arm. The copper gasket is compressed using the six bolt holes originally part of the flanges, creating a

vacuum seal. The six bolt holes are recessed on one side of the vacuum seal disc so that the probe head can mount flush with its surface, without the bolt heads interfering. The wires on the vacuum side are also trimmed to length (less than the spacer ring thickness) so that they do not collide with the collector. Three additional holes are drilled through both flanges to accept the #4 mounting screws from the GEA probe head.

The availability of only four wires in the electrical feedthrough limits the opportunity for future expansion of the Mochi.GEA. All of these wires are currently in use for the repeller grids, collector, and a secondary electron suppressor. However, it is not common to have more than four powered/measured GEA components, so this will likely not pose a significant issue.

The engineering drawings of these components can be found in Appendix A.

3.6 Assembly & Checkout Testing

Prior to assembly all parts are carefully cleaned in preparation for high vacuum. The GEA probe head is then assembled using the mounting screws as guides. This allows the grids/collector and electrical contacts to be laid into the shelf and the next insulation ring stacked on top, as shown in Figure 7. The probe arm and vacuum seal are then suspended just above the stack and the lead wires are trimmed and soldered to the feedthrough wires. A multimeter is then used to verify the electrical connection from each electrical contact's copper ring back to the inner conductor of its BNC on the electronics enclosure. The probe arm is then lowered and mounted to the probe head stack.

A few checkout tests are then performed to ensure that the assembly is in working condition. First, a BNC cable is used to connect the forward-most grid to a power supply and a potential is applied. The multimeter is then used to measure the potential of this grid with respect to the probe arm, being careful not to damage the grid. Next, a second power supply is connected to the next grid using a BNC cable. A large potential difference is then applied between the grids to determine if there is a short in the system or arcing between the grids. The assembly can stand off at least 500V between the grids with < 2mA of leakage current. The final checkout test is to install the probe on the chamber and verify its vacuum integrity. To date the Mochi.GEA has

been pumped down to about $2x10^{-6}$ torr, which is equal to the base pressure of the vacuum chamber without the probe installed.

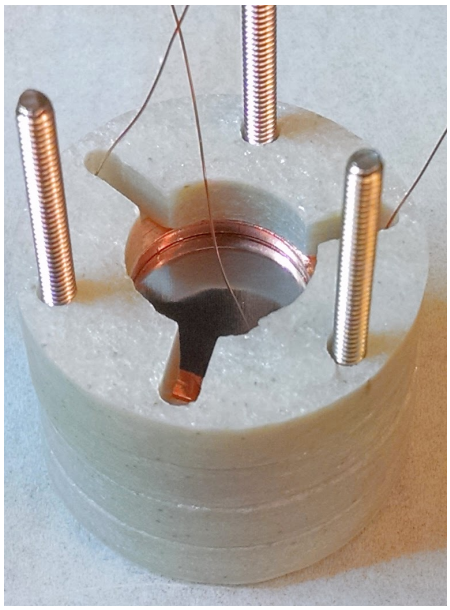

Figure 7. Photograph of Mochi.GEA probe head during assembly, showing the spacer ring, collector and its electrical contact.

4 DISCUSSION OF RESULTS

The GEA was tested on several occasions over the course of about two and a half months, measuring about 850 shots in total. The intent of these tests was to try many different electrical and mechanical configurations in an attempt to troubleshoot the probe. The GEA was tested in two locations: about 20cm from the edge of the outer electrode of the Mochi.SpheromakGun, and on the Mochi.LabJet Gun port. The first location (shown in Figure 8) is close to the plasma and nearly perpendicular to the axis of the jet. The second is aligned with the axis of the jet but on the opposite side of the chamber (about 1.4m away).

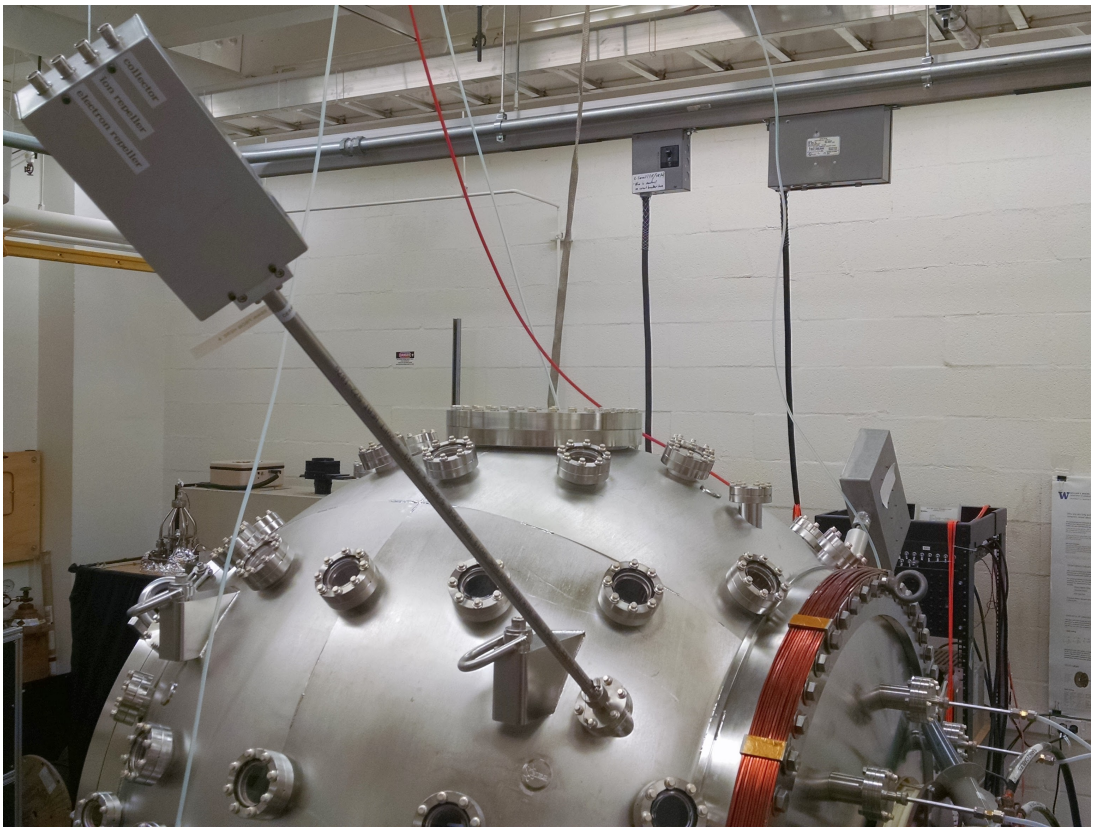

Figure 8. Photograph of the Mochi.GEA installed on the vacuum chamber near the .SpheromakGun.

The following sections describe the major results of these tests and are not necessarily presented in chronological order.

4.1 Subtraction of Reference Potential

The electrical configuration of the GEA is perhaps the most easily modified part of the design and many different configurations were tested. The use of attenuators, 50Ω terminators and DC vs. AC coupling of the oscilloscope had little effect on the measured signal. Using insulated BNC connectors introduced capacitively-coupled noise into the signal, so the current circuit has grounded connectors for the oscilloscopes and power supplies. This requires the oscilloscope and supplies to be plugged in using cheater plugs, in order to avoid ground loops, as discussed in section 3.2. The GEA collector signal was fairly repeatable across all of these variations.

It is possible that the GEA collector signal is superimposed upon other signals (e.g., gun current or voltage), from which it inherits its repeatability. It is shown in the circuit diagram in Figure 2 that the collector signal is referenced to the vacuum chamber, which is connected experiment ground. The reference potential for pulsed, high-power experiments often floats throughout a pulse, as it is not a perfect ground. It certainly likely that the Mochi vacuum chamber will float as the -4kV capacitor banks are discharged to it. For this reason, the GEA collector signal is the sum of the signal due to the plasma and the floating reference potential of the chamber.

This is further suggested by Figure 9, which shows a collector signal where the probe was pulled all the way back to the chamber wall, and another collector signal with the probe pushed forward by 10cm. Moving the probe closer to the plasma seems to have two effects: the amplitude of the signal increases and the signal rises about 100μs earlier. A difference of 100μs and 10cm corresponds to a sped of about 1km/s, which is a reasonable speed at which the plasma could propagate across the chamber. This time-of-flight estimation supports the conclusion that some portion of the signal is due to the plasma itself. However, it is also clear from this plot that the signal begins to rise at about 10μs, the time of plasma breakdown, and too early to represent the plasma reaching the probe head (about 1.4m away). This part of the signal must be due to the reference potential of the measurement (chamber potential) falling rapidly, which is consistent with the plasma effectively shorting the chamber to the -4kV capacitor bank.

Referencing the GEA collector measurement do a different ground could be dangerous with the experiment ground floating. This means that the floating chamber signal will always be a part of the measurement, and it must be removed in order to retrieve only the signal due to the plasma. This is currently done using the fourth BNC connector, connected to channel A of the oscilloscope as depicted in the circuit diagram in Figure 2. The reference potential of this BNC cable fluctuates like that of the GEA collector but ideally does not measure any other signal, allowing it to be subtracted from the GEA collector signal as shown in Figure 10.

With the exception of Figure 13, all following results are shown without the floating reference potential subtracted.

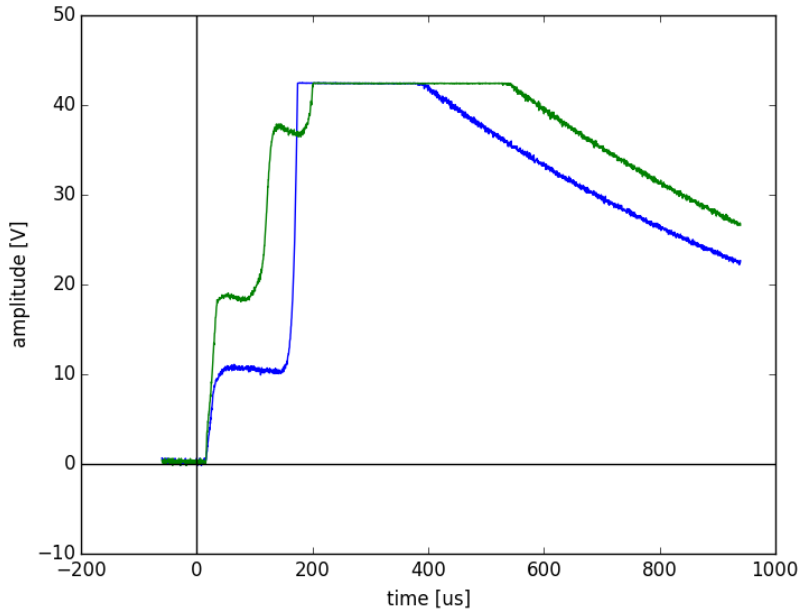

Figure 9. GEA collector signals with the probe at minimum depth (blue, shot 1602) and pushed in by 10cm (green, shot 1604). *Repeller potentials: -46V / +80V; gate open; location: .LabJet Gun; without aperture; without secondary electron suppressor*.

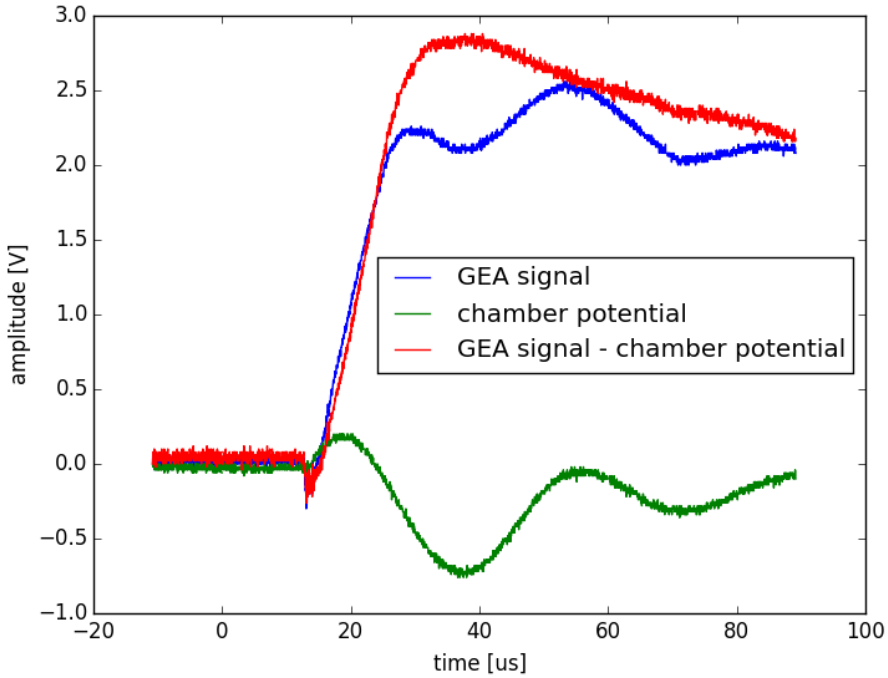

Figure 10. The GEA collector signal and chamber potential signal to which the GEA is referenced (shot 1773). Subtracting the chamber potential signal from the GEA signal provides a clean result. *Repeller potentials: -46V / +70V; gate open; probe depth: minimum; location: .LabJet Gun; with aperture; without secondary electron suppressor*.

4.2 Indication of Excessive Flux & Space Charge Limitation

The initial GEA collector signals were characterized by very large amplitude (up to 40V) and large negative spikes. The large signal amplitude indicates that the collected flux was much higher than expected. It has been shown on other GEAs that there is a limit to the amount of current that can be driven to the device without encountering space charge issues. Large, negative current spikes have been observed above this threshold [1]. Moving the GEA to the opposite end of the vacuum chamber, 1.4m farther away, did not solve the issue, as can be seen in Figure 11. The shots pictured in Figure 9 above, which do not have the negative current spikes, were actually taken with the gate nearly closed. This indicated that the plasma flux to the probe needed to be significantly reduced.

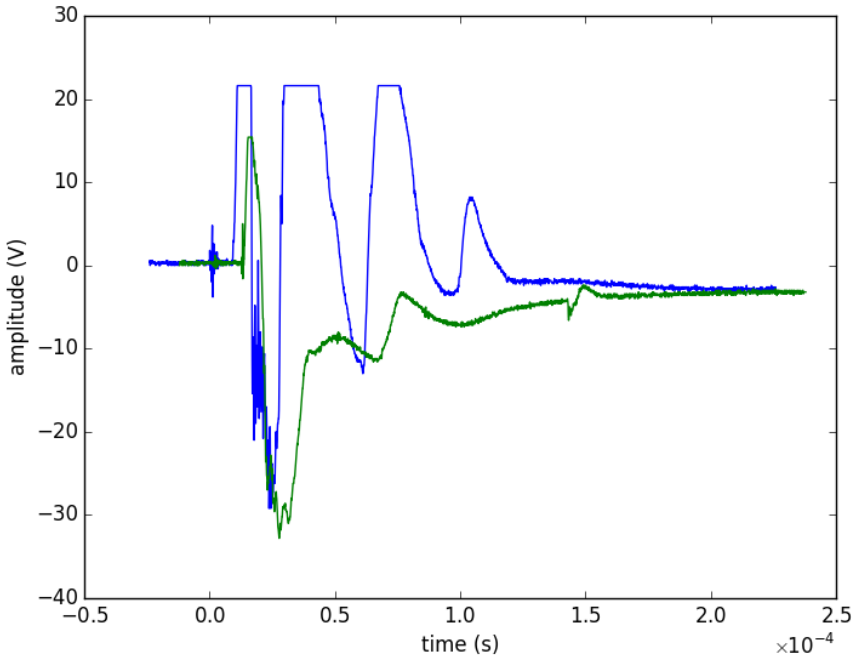

Figure 11. GEA collector signals at the .SpheromakGun location (blue, shot 1364) and the .LabJet Gun location (green, shot 1445), showing large signal amplitude and negative current spikes at 25µs. *Repeller potentials: -60V / +50V; gate open; probe depth: minimum; without aperture; without secondary electron suppressor.*

In order to limit the flux an aperture was designed and installed on the Mochi.GEA, as pictured in section 3.4.5. Ideally, this aperture would limit the flux to the device to just below the space charge limitation threshold. Estimating the threshold flux can be difficult and requires

knowledge of the plasma parameters [1]. Furthermore, this threshold varies with location in the vacuum chamber. For this reason, the aperture was designed to limit the flux as much as possible but allow for future adjustment, as discussed in section 3.4.5. This aperture corresponds to about a 26x reduction in solid angle and a 17x reduction in open area. As shown in Figure 12, this reduced the peak signal amplitude by a significant amount (about 56x for the signals shown). Observed over many shots it was clear that this removed the large negative spikes that indicate space charge limitation from the signal.

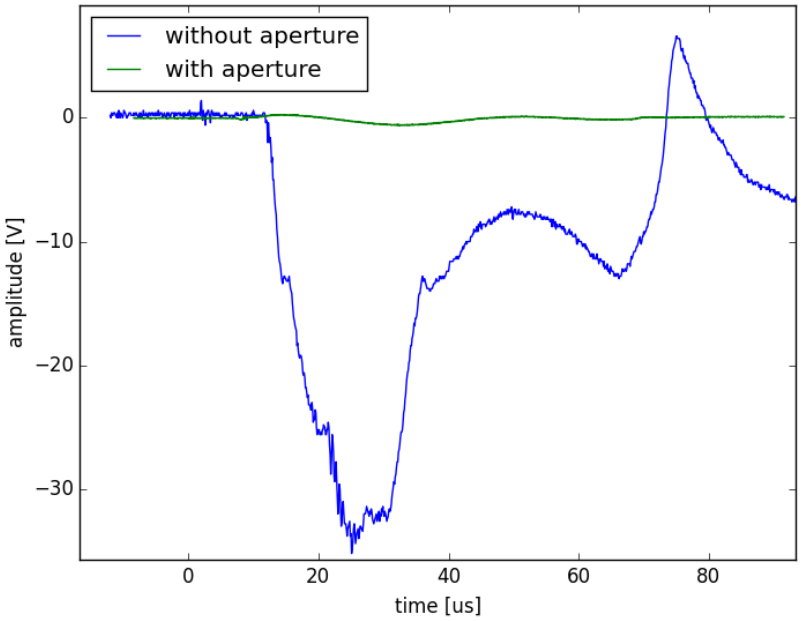

Figure 12. GEA signals without the aperture (blue, shot 1437) and with the aperture installed (green, shot 1637). *Repeller potentials: -60V / +0V; gate open; probe depth: minimum; location: .LabJet Gun; without secondary electron suppressor*.

4.3 Effect of Outgassing of Probe Head

During initial testing with the aperture installed it was observed that the signal seemed to increase in amplitude over successive shots. This was tested in various GEA states by taking consecutive shots with the minimum possible time between shots (about 3 minutes), followed by a The peak of the signal increased for each shot until the break, after which the signal returns to its original amplitude. Between shots the repelled ions and electrons may recombine to form neutral gas within the probe head. If this gas is not adequately pumped out it may interact with

the incident plasma during the next shot, to provide additional current. It is possible that the aperture limits the ability of the probe head to be pumped out.

The pumpout time of the probe head can be estimated using the equations for pumpout and conductance of molecular flow through a cylindrical hole [1]:

$$t = \frac{V\alpha \ln(\alpha)}{C(\alpha - 1)} \qquad \text{and} \qquad C = \sqrt{\frac{\pi kT}{2m}} \frac{d^3}{4d + 3l} \tag{8}$$

where t is pumpout time, V is probe head volume, $\alpha = p/p_0$ is the ratio of peak pressure during a shot to desired baseline pressure, C is the conductance through the hole, kT is the probe operating temperature in eV, m is the ion species mass, d is the aperture hole diameter, and l is the length of the aperture hole. The interior of the probe head has a radius of about 8mm and a length of about 19mm (three 0.25in thick insulation rings), giving rise to a volume, V, of about 3.8×10^{-6}m. The gas species used for these shots was diatomic nitrogen, so m is assumed to be 28 proton masses in eV/c^2. The diameter and length of the aperture hole are 0.9mm and 6.35mm, respectively. Using an α of 30 and an operating temperatures of 20-200°C, the maximum estimate of pumpout time was 0.6s, much less than the time between shots of 3 minutes.

Prior to observing this effect the chamber had been at atmosphere for over a week and was brought up without the use of a nitrogen purge, possibly allowing water to condense into the probe head. In order to investigate this as a cause, additional testing was performed after the probe head and chamber had been at about 3×10^{-6} torr for 17 days. During this testing no increase in signal amplitude over successive shots was observed, consistent with the above estimate of pumpout time. For this reason it is believed that the observed increase was due to outgassing of the probe head components, not inadequate pumpout with the aperture installed. This effect is important to note for future testing.

4.4 Indication of Secondary Electron Emission Issue

Before the aperture was installed, shots 1463-1482 showed that a positive pulse existed in the GEA collector signal on the millisecond timescale, hundreds of times longer than the life of the plasma. This feature of the measured signal appeared to directly follow the ion repeller potential

imposed with the power supply (the collector and ion repeller grid were properly electrically isolated). This feature persisted even after the aperture was installed to limit the plasma flux, indicating that this direct coupling could be caused by secondary electron emission: as the ion repeller potential is increased, the grid draws more secondary electrons off of the collector, leading to a larger amplitude signal.

Secondary electron emission is a common problem with GEAs, and the common solution is to add a grid in between the ion repeller and collector to act as a secondary electron suppressor. This grid is biased to a negative potential to push the secondary electrons back to the collector, negating their current. A secondary electron suppressor grid was added to the Mochi.GEA and connected to an array of batteries inside the electronics enclosure via an ON/OFF switch. When turned on the suppressor is biased to -52V, although this can be easily changed by changing the batteries. The result of the secondary electron suppressor can be se seen in Figure 13 below. This clearly reduces the amplitude of the signal and removed the direct coupling to the ion repeller, indicating that secondary electron emission was the issue.

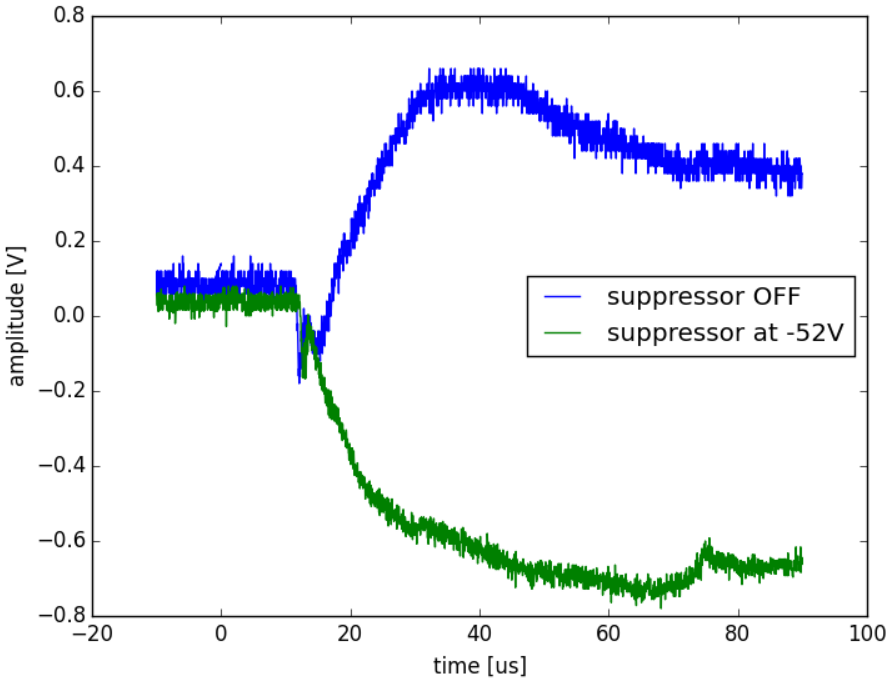

Figure 13. GEA signals of shot 1869 with the secondary electron suppressor off (blue) and shot 1886 with the suppressor at -52V (green). *Repeller potentials: -46V / +70V; gate open; probe depth: minimum; location: .LabJet Gun; with aperture*.

4.5 Estimation of Electron Energy Distribution & Temperature

When it was decided that the flux to the probe should be limited, a series of shots was taken with the gate closed. With the ion repeller at 0V and the electron repeller at -10V, the signal looked like a negative current pulse. When the electron repeller potential was decreased, the amplitude of the signal decreased as well. This indicated that the closed gate was effectively blocking the ions, while the more mobile electrons were flowing around it and into the device (the gate does not provide a perfect seal, as pictured in Figure 4). These electrons were then partially repelled, so that the GEA was effectively working in "electron mode". These signals, corresponding to electron repeller potentials from -10V to -320V, are shown in .

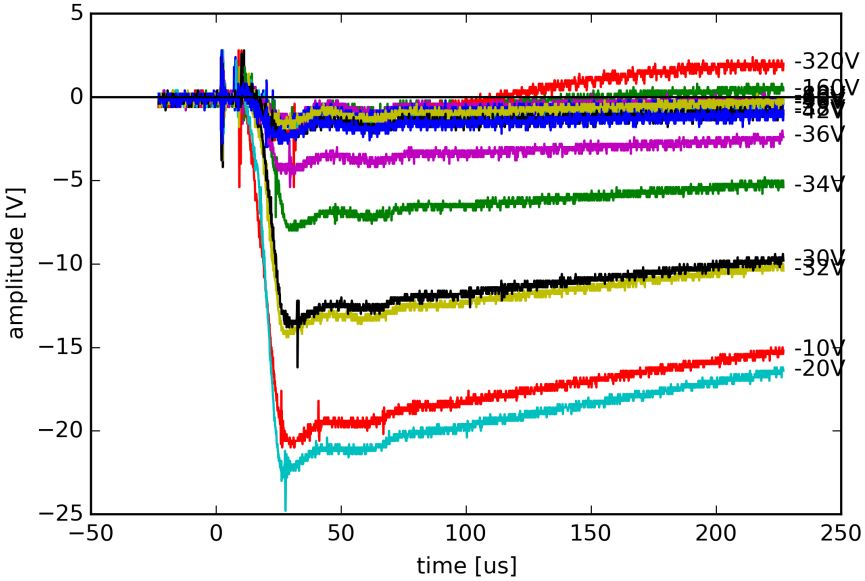

Figure 14. Collector measurements with the gate closed at various electron repeller potentials used to determine the electron energy distribution. *Ion repeller potential: +0V; probe depth: minimum; location: .LabJet Gun; without aperture; without secondary electron suppressor*.

These signals served as prototype data during development of the computational procedure for future analysis of ion data. They also provided the opportunity to estimate the electron energy distribution and temperature in this location with the gate closed. The analysis was performed in Python and is shown in full in Appendix B. The results of the analysis are shown in and below. The electron energy distribution appears to be Maxwellian, although the distribution is negative

at some energies (corresponding to points of positive slope on the I-V curve). This is not consistent with the definition of the distribution being the number of particles per unit energy. This could be caused by an effect like secondary electron emission, but it is more likely the result of shot-to-shot variability. This particular analysis is under sampled (only one measurement was taken at each repeller potential) and it is possible that distribution would be entirely positive if averaged over several shots at each repeller potential.

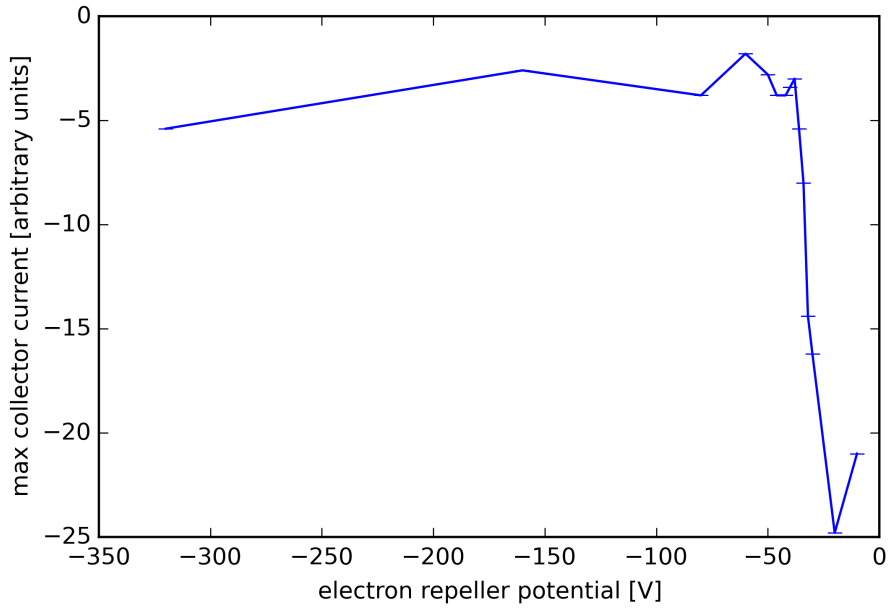

Figure 15. Estimate of I-V characteristic, as measured in electron mode.

A Maxwellian energy distribution was fitted to the measured *g(E)*, as shown in . This Maxwellian suggests that the electron temperature in this location is 5eV and is also shifted in energy by 20eV. This shift indicates that the particles enter the device at 20eV below the collector potential (0V in this case). Since these shots were taken with the gate closed, the shift is related to the plasma potential in a complicated way. Determining the plasma potential from this shift would require knowledge of the sheath structure around the gate, as well as its floating potential. Had these shots been taken with the gate open or with the ceramic aperture installed (see section 1.1), this shift would provide a direct estimate of the plasma potential.

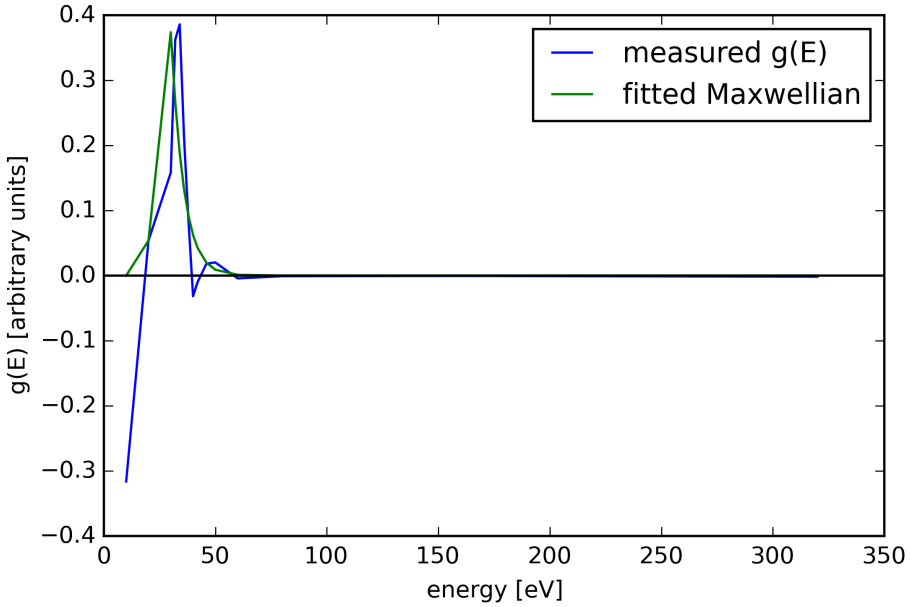

Figure 16. Estimate of the electron energy distribution, *g(E)*. The negative portion of the distribution is likely due to shot-to-shot variability. The fitted Maxwellian indicates an electron temperature of 5eV and a shift of 20eV.

4.6 Possible Remaining Issues

The addition of the secondary electron suppressor is the most recent design modification to the Mochi.GEA at the time of this thesis. With the suppressor turned on, the ability to control the shape and amplitude of the signal with the repeller grids is limited. All signals are negative, with a peak of about -1V, and last for at least 100μs, like that shown in Figure 13 above. The positive uptick in the signal before 80μs is not controllable with the ion repeller and does not occur earlier in the signal when the probe depth is increased; thus it is likely that this feature is not due to ions arriving at the device. For this reason, the Mochi.GEA has yet to observe a controllable, positive current pulse associated with the arrival of ions, and the ion energy distribution has yet to be determined.

It is possible that the signal shape described above is the result of ineffective shielding by the insulation rings. Small pieces of ceramic material occasionally flaked off of the rings during machining, possibly leaving small voids in the shielding. If mobile electrons are allowed to flow through these voids into the probe head between the secondary electron suppressor and collector,

they would be pushed toward the collector and give rise to a negative current. This issue could be addressed by surrounding the probe head with a shield or modifying the insulation rings to overlap with each other and provide better shielding.

Another possible issue is that the grid hole size (0.48mm) is too large compared to the plasma Debye length. This could cause the applied repeller potentials to be shielded, allowing some of the plasma to pass through the device unhindered. This issue may be addressed by making or purchasing custom grids with a smaller hole size. However, appropriate design of new grids to combat this issue would require knowledge of the Debye length, which is not available at this time.

Finally, the lack of a clear ion signal may simply be the result of lack of ion flux. It is possible that the current aperture hole size may reduce the flux too drastically, so that other effects obscure the ion current signal. The aperture hole size may need to be increased, at the risk of re-introducing space charge limitation issues. Also, the space charge limitation threshold may be increased by applying a negative bias to the collector [1]. However, it may be appropriate to address effects like shielding against mobile electrons prior to increasing the aperture hole size, as this may clean up the signal.

5 CONCLUSION

At this time, the Mochi.GEA has not observed a positive ion current pulse that can be attenuated using the ion repeller grid. However, the simple design of the device has allowed modifications that have mitigated several issues. The first major issue was that the particle flux to the device was very large, exceeding the threshold current density for onset of space charge issues. This was associated with large, negative current spikes in the collector signal. The installation of a pinhole aperture limited the particle flux, removing this unwanted feature from the signal. However, as an ion current signal has not been observed, it may be necessary to increase the aperture hole size and negatively bias the collector to increase the space charge limitation threshold.

Another issue observed throughout testing was that of direct coupling of the collector signal to the ion repeller grid potential. Increasing the repeller potential increased the amplitude of the signal, whereas it is expected to repel ions and thus decrease the amplitude. This issue may have been exacerbated by the large particle flux in the pre-aperture tests, but its root cause was secondary electron emission from the collector. When the repeller potential was increased, the grid more rapidly drew secondary electrons off of the collector surface, which corresponds to a positive current. The addition of a secondary electron suppressor effectively removed this unwanted feature from the signal. However, this suppressor also limits the ability of the repeller grids to control the signal, suggesting that it may be pushing electrons that leak into the device toward the collector. It may be necessary to better shield the probe head from these mobile electrons.

The GEA is referenced to experiment ground, which fluctuates repeatably during a shot. Many iterations of the GEA circuit diagram were tested in an attempt to remove noise and this reference potential fluctuation from the signal. The current circuit design measures this floating potential and allows it to be subtracted from the signal for a clean result. A more sophisticated circuit design may be investigated in the future, but the prominent issues with the current signal are likely not related to the circuit design.

Perhaps the most promising result thus far is the ability to estimate the electron energy distribution and temperature. This was done far away from the plasma gun and using the gate to block ions from entering the device, while allowing a small amount of more mobile electrons to enter. This analysis served as a prototype for future analysis of ion data, and allowed for the development of an analysis procedure using Python. This also suggests that the Mochi.GEA may be capable of measuring the ion and electron energy distribution function of plasmas if the flux to the device can be tailored to maximize signal without causing space charge issues. This warrants continued development of the probe.

BIBLIOGRAPHY

[1] Pitts, Chavan, Davies, Erents, Kaveney, Matthews, . . . Duran. (2003). “Retarding field energy analyzer for the JET plasma boundary”. *Review Of Scientific Instruments, 74*(11), 4644-4657.

[2] A. L. Moser and P. M. Bellan. (2012). “Magnetic reconnection from a multiscale instability cascade.” *Nature*, 482(7385), 379.

[3] C. Böhm and J. Perrin. (1993). “Retarding-field analyzer for measurements of ion energy distributions and secondary electron emission coefficients in low-pressure radio frequency discharges”. *Review of Scientific Instruments, 64*, 31.

[4] I. Hutchinson. (2002). *Principles of plasma diagnostics* (2nd ed.). Cambridge; New York: Cambridge University Press.

[5] U. Shumlak and T. Maruo. (2006). "Plasma Plume Mass Characterization of a Mini-pulsed Plasma Thruster." *Collection of Technical Papers - AIAA/ASME/SAE/ASEE 42nd Joint Propulsion Conference* 1: 279-93.

[6] T. A. Burton. (2002). “Exhaust Plume Characterization of a Mini-PPT Using a Time-of-Flight/Gridded Energy Analyzer,” M. S. Thesis, University of Washington.

APPENDIX A – ENGINEERING DRAWINGS

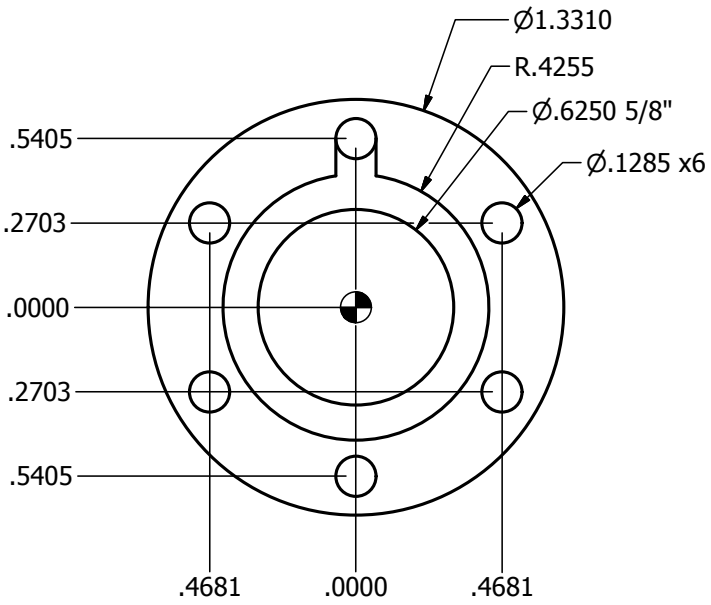

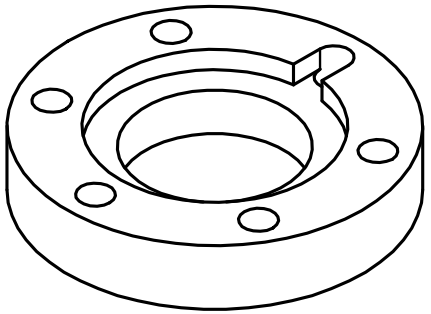

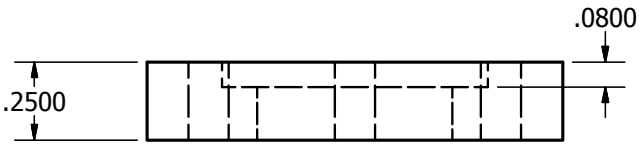

Part: MOCHI.GEA Grid Insulation Ring
Designed by: Morgan Quinley

Units: inches (for use in machine shop)
Scale: 2 to 1

Material: Mykroy/Mycalex ceramic

Notes:

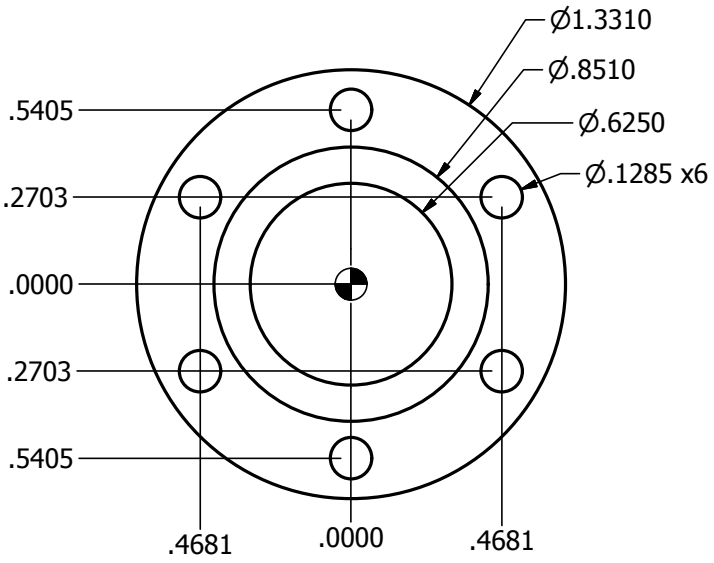

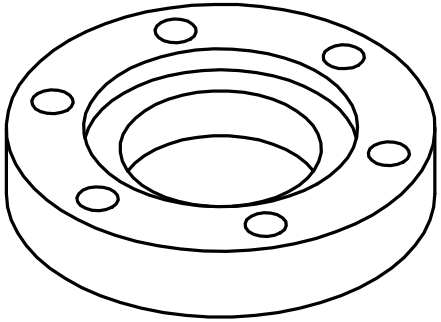

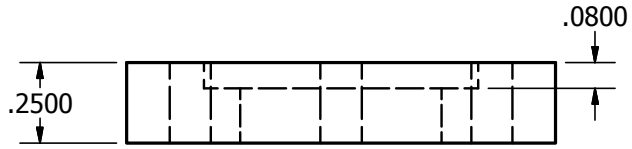

Part: MOCHI.GEA Collector Insulation Ring
Designed by: Morgan Quinley

Units: inches (for use in machine shop)
Scale: 2 to 1

Material: Mykroy/Mycalex ceramic

Notes:
This part is the same as the MOCHI.GEA Grid Insulation Ring without the small channel for the lead wire.

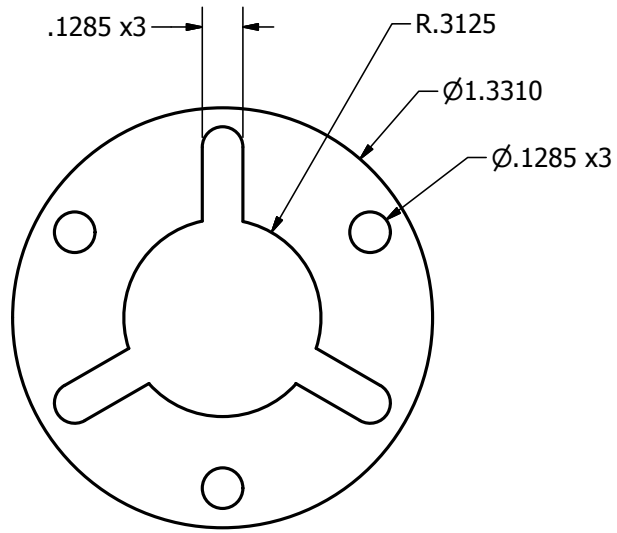

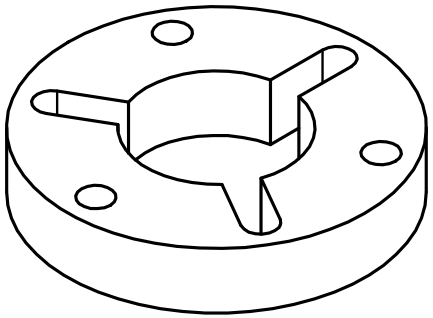

Part: MOCHI.GEA Spacer Ring
Designed by: Morgan Quinley

Units: inches (for use in machine shop)
Scale: 2 to 1

Material: Mykroy/Mycalex ceramic

Notes:

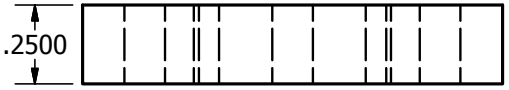

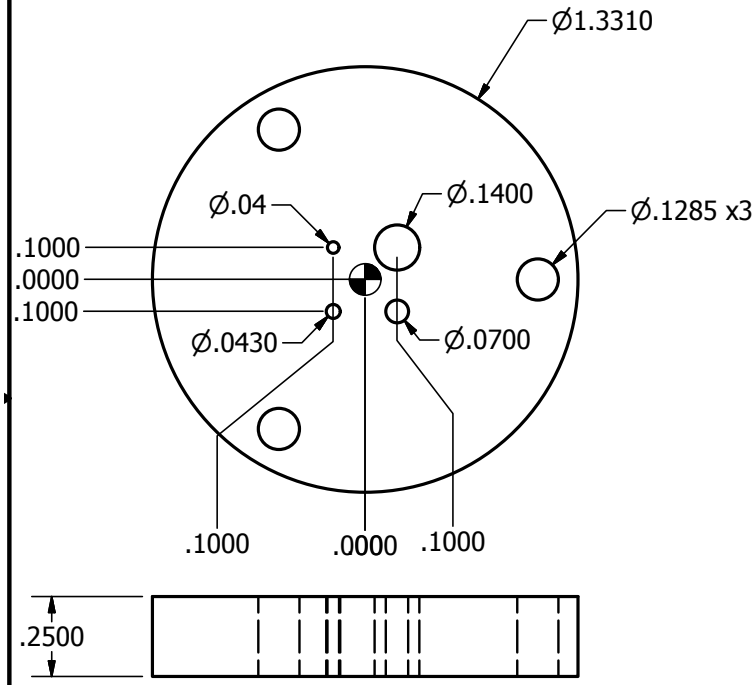

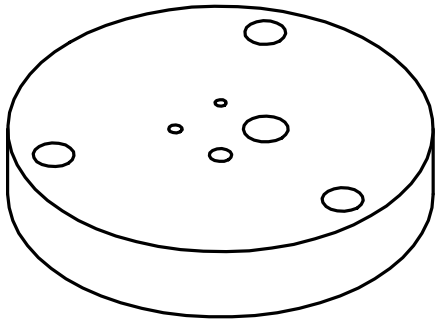

Part: MOCHI.GEA Aperture
Designed by: Morgan Quinley

Units: inches (for use in machine shop)
Scale: 2 to 1

Material: Mykroy/Mycalex ceramic

Notes:
This aperture was machined with the 4 holes shown, but before testing the three larger holes were filled with Torr Seal. These may be drilled out in the fiture to increase the aperture hole size.

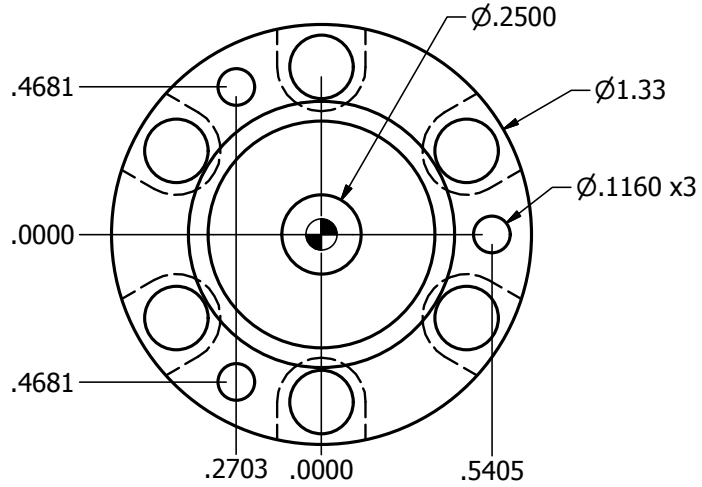

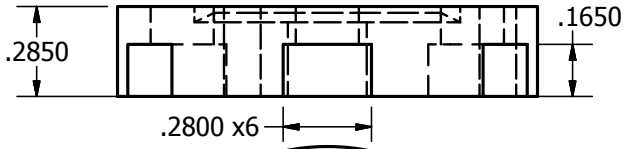

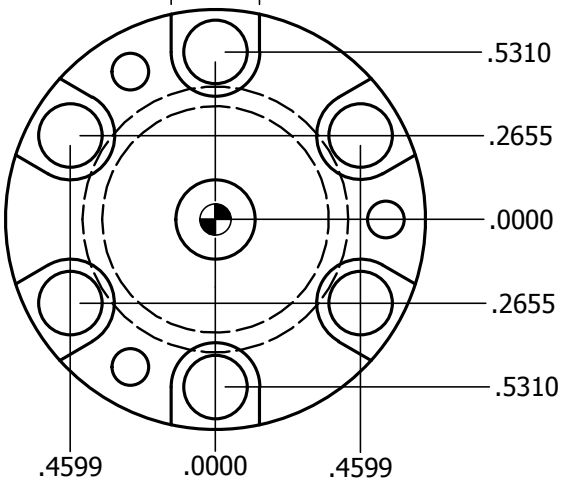

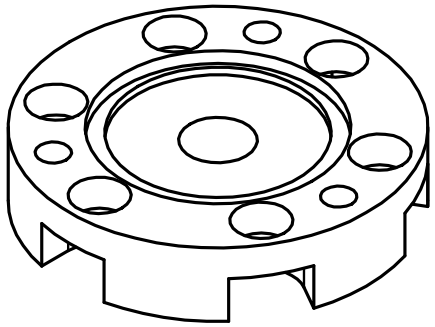

Part: MOCHI.GEA Vacuum Seal Disc
Designed by: Morgan Quinley

Units: inches (for use in machine shop)
Scale: 2 to 1

Material: stainless steel

Notes:
This part is a modified 1-1/3" CF vacuum flange. Not all original geometry is dimensioned here; see the standard part for other dimensions.

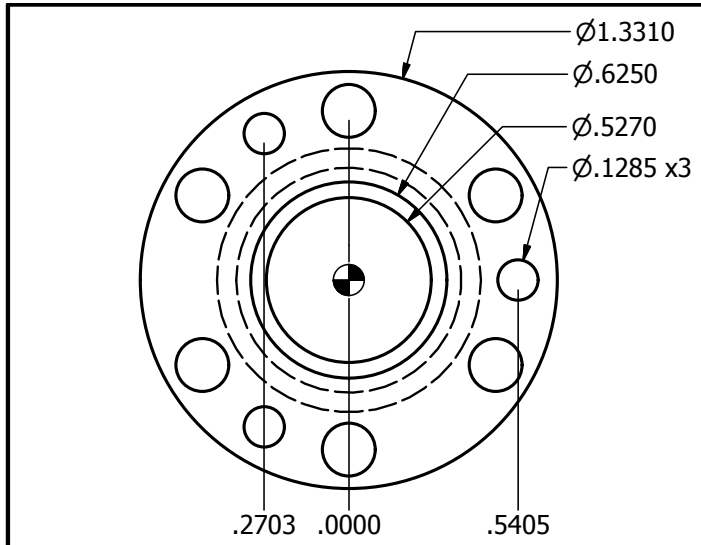

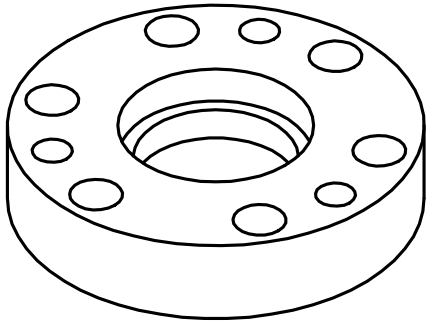

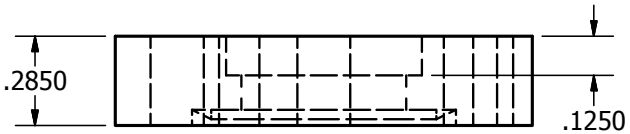

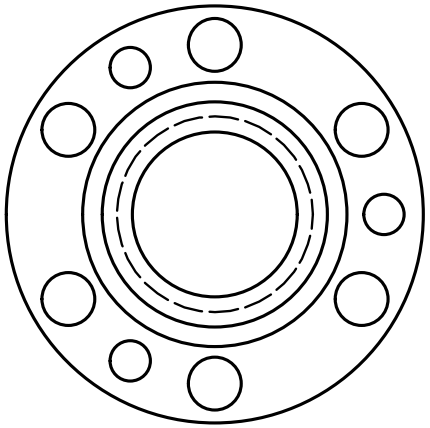

Part: MOCHI.GEA Probe Arm Flange
Designed by: Morgan Quinley

Units: inches (for use in machine shop)
Scale: 2:1

Material: stainless steel

Notes:
This part is a modified 1-1/3" CF vacuum flange. Not all original geometry is dimensioned here; see the standard part for other dimensions.

This part is welded to a 5/8" OD stainless steel tube to make the MOCHI.GEA probe arm

APPENDIX B – ELECTRON DATA ANALYSIS

Goal

The primary goal of this analysis is to estimate the electron energy distribution, temperature, and plasma potential of the Mochi.SperomakGun plasma using Mochi.GEA data from shots 1524 - 1538 (taken on 16 July 2015). During these shots the GEA was installed on the Mochi.LabJet Gun port and all shots were taken at the minimum probe depth with the gate closed. It was found during these shots that decreasing the electron repeller potenial decreased the amplitude of the negative signal. This indicated that the GEA was operating in "electron mode", allowing the electron energy distribution in this state to be determined.

Another goal is to aid in development of the Mochi.GEA data analysis method. This notebook may serve as a template for future analysis of Mochi.GEA data. This notebook can be found on the MochiLab/Mochi.GEA_electron_analysis repository on Bitbucket.

Data analysis method

- Create a python dictionary containing relevant shot information
- Import data into the dictionary using import_from_scope.py
- Plot all traces, labeled with their electron repeller potential (this may be infeasible with many shots)
- Determine peak current (or total collected charge) for each shot and add it to the dictionary
- Collect all of the peak current (or total collected charge) data points by electron repeller potential
- Calculate the mean and standard deviation for each electron repeller potential
- Plot the mean and standard deviation versus electron repeller potential (I-V curve)
- Differentiate the I-V curve and multiply by appropriate scaling to determine distribution function g(E)
- Plot g(E)
- Fit an energy Maxwellian to g(E) and use the fit parameters to estimate temperature and plasma potential

Possible improvements

- If there are many shots to be analyzed in the future, manually setting up the dictionary may be tedious. Instead it may be appropriate to import the relevant information for each shot from a Mochi.GEA shot log (text file or spreadsheet).
- When plotting the signals spread the annotations out (maybe use arrows) to make it more readable; this may not be necessary because this plot may be too cluttered when there are multiple signals per repeller potential.
- Consider using python's Pandas library instead of dictionaries.
- Perform error analysis to estimate systematic error and propagate it throughout the analysis.
- Plot the I-V characteristic and g(E) with error bars equal to systematic error plus shot-to-shot variability (standard deviation of peak currents at a each potential). Also plot without a line connecting the means, but instead see if the fit passes through the error bars.

Analysis

Initializing the shot information dictionary

In [1]:
```
shot_data = {'shot_1524' : {'shot_#' : 1524, 'filename' : '1524.cs
v', 'channel' : 'CH4', 'phi_e' : -10.,  'phi_i' : 0.},
             'shot_1525' : {'shot_#' : 1525, 'filename' : '1525.cs
v', 'channel' : 'CH4', 'phi_e' : -20.,  'phi_i' : 0.},
             'shot_1526' : {'shot_#' : 1526, 'filename' : '1526.cs
v', 'channel' : 'CH4', 'phi_e' : -40.,  'phi_i' : 0.},
             'shot_1527' : {'shot_#' : 1527, 'filename' : '1527.cs
v', 'channel' : 'CH4', 'phi_e' : -80.,  'phi_i' : 0.},
             'shot_1528' : {'shot_#' : 1528, 'filename' : '1528.cs
v', 'channel' : 'CH4', 'phi_e' : -160., 'phi_i' : 0.},
             'shot_1529' : {'shot_#' : 1529, 'filename' : '1529.cs
v', 'channel' : 'CH4', 'phi_e' : -320., 'phi_i' : 0.},
             'shot_1530' : {'shot_#' : 1530, 'filename' : '1530.cs
v', 'channel' : 'CH4', 'phi_e' : -60.,  'phi_i' : 0.},
             'shot_1531' : {'shot_#' : 1531, 'filename' : '1531.cs
v', 'channel' : 'CH4', 'phi_e' : -50.,  'phi_i' : 0.},
             'shot_1532' : {'shot_#' : 1532, 'filename' : '1532.cs
v', 'channel' : 'CH4', 'phi_e' : -30.,  'phi_i' : 0.},
             'shot_1533' : {'shot_#' : 1533, 'filename' : '1533.cs
v', 'channel' : 'CH4', 'phi_e' : -32.,  'phi_i' : 0.},
             'shot_1534' : {'shot_#' : 1534, 'filename' : '1534.cs
v', 'channel' : 'CH4', 'phi_e' : -34.,  'phi_i' : 0.},
             'shot_1535' : {'shot_#' : 1535, 'filename' : '1535.cs
v', 'channel' : 'CH4', 'phi_e' : -36.,  'phi_i' : 0.},
             'shot_1536' : {'shot_#' : 1536, 'filename' : '1536.cs
v', 'channel' : 'CH4', 'phi_e' : -38.,  'phi_i' : 0.},
             'shot_1537' : {'shot_#' : 1537, 'filename' : '1537.cs
v', 'channel' : 'CH4', 'phi_e' : -42.,  'phi_i' : 0.},
             'shot_1538' : {'shot_#' : 1538, 'filename' : '1538.cs
v', 'channel' : 'CH4', 'phi_e' : -46.,  'phi_i' : 0.}}
```

This creates a dictionary of shots. Each shot is a dictionary of information associated with it. The variables phi_e and phi_i are the electron and ion repeller potentials, respectively. Information for a shot is retrieved by calling shot_data[shot name][desired information]. For example:

In [3]:
```
print 'The electron repeller potential for shot 1528 is', shot_dat
a['shot_1528']['phi_e'], 'V'
print 'The oscilloscope channel for shot 1534 is', shot_data['sho
t_1534']['channel']
```

```
The electron repeller potential for shot 1528 is -160.0 V
The oscilloscope channel for shot 1534 is CH4
```

Importing the raw data

The next cell imports a python module that processes oscilloscope raw data, given a filename and oscilloscope channel. This script is available in the MOCHILab/import_from_scope repository on Bitbucket.

In [4]:
```
import sys
sys.path.append('/Users/mjquinley/repositories/import_from_scope/')
import import_from_scope
```

The next cell creates a new key called 'signal' for each shot in the shot_data dictionary and populates it with a python tuple containing two Numpy arrays: the time data in element 0 and the amplitude data in volts in element 1.

In [5]:
```
for shot_name in shot_data:
    shot_data[shot_name]['signal'] = import_from_scope.main(shot_da
ta[shot_name]['filename'],
                                                            shot_da
ta[shot_name]['channel'])
```

Plotting the raw data

In [8]:
```
# Set up the plotting module
%matplotlib inline
import matplotlib.pyplot as plt
```

The next cell iterates on the shot data to plot amplitude versus time for each signal.

In [21]:
```
for shot_name in shot_data:
    time      = shot_data[shot_name]['signal'][0]
    amplitude = shot_data[shot_name]['signal'][1]
    plt.plot(time*1e6, amplitude, label=shot_data[shot_name]['ph
i_e'])
    # The next statement shows the electron repeller potential at t
he end of the signal
    plt.annotate(str(int(shot_data[shot_name]['phi_e']))+'V',
                 (shot_data[shot_name]['signal'][0][-1]*1e6, shot_d
ata[shot_name]['signal'][1][-1]),
                 xytext=(5,-2), textcoords='offset points'
                )
plt.xlim(-50,270)
plt.axhline(color='black')  # adds a horizontal black line at ampli
tude = 0
plt.xlabel('time [us]'), plt.ylabel('amplitude [V]')
plt.savefig('signals_to_be_analyzed.png', dpi = 400)
plt.show()
```

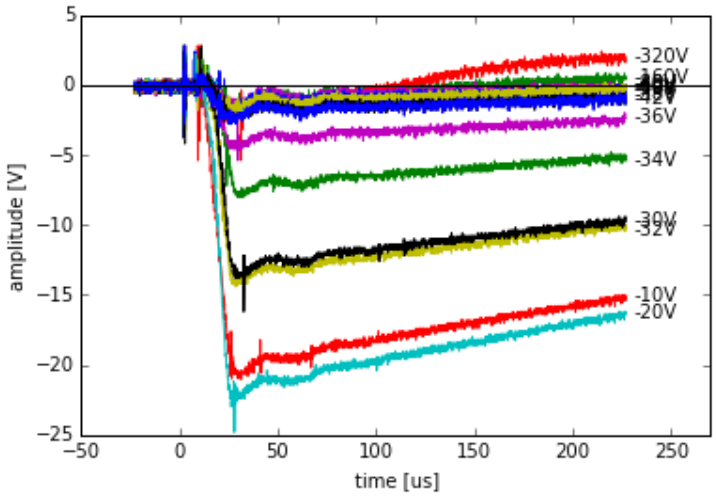

The traces for phi_e = -320V and phi_e = -160V go positive after 100us. This is likely due to an effect like secondary electron emission. These signals may need to be removed from the analysis.

An alternate, and perhaps cleaner, method of labeling the traces using a legend is:

plt.legend(title='electron repeller potential [V]', loc='upper left', ncol=2, bbox_to_anchor=(1.025, 1), borderaxespad=0.)

But this requires the signals to be plotted in order by phi_e (which is difficult because items are retrieved from dictionaries at random) and plotted with non-repeating colors. This may be investigated in the future. However, this plot may be infeasible in the future, because there will be many shots for each repeller potential.

Determining the peak collector current

The next cell determines the peak collector current for each signal. Note that there are spikes near the peak in some signals, which may need to be removed by filtering. However, a more statistically appropriate method of removing these spikes is to take several shots at each potential and determine the average peak current.

In [22]:
```
for shot_name in shot_data:
    amplitude = shot_data[shot_name]['signal'][1]  # signal amplitude in arbitrary units
    Ic_peak  = amplitude.min()  # peak current in arbitrary units
    shot_data[shot_name]['Ic_peak'] = Ic_peak  # assigns Ic_peak to shot_data dictionary
```

NOTE: the use of .min( ) in the cell above is specific to electron data. This must be changed to .max() when analyzing ion data.

In [23]:
```
print 'shot 1525:', 'phi_e =', shot_data['shot_1525']['phi_e'], ', Ic_peak =', shot_data['shot_1525']['Ic_peak']
print 'shot 1534:', 'phi_e =', shot_data['shot_1534']['phi_e'], ', Ic_peak =', shot_data['shot_1534']['Ic_peak']
print 'shot 1528:', 'phi_e =', shot_data['shot_1528']['phi_e'], ', Ic_peak =', shot_data['shot_1528']['Ic_peak']
print 'shot 1529:', 'phi_e =', shot_data['shot_1529']['phi_e'], ', Ic_peak =', shot_data['shot_1529']['Ic_peak']
```

```
shot 1525: phi_e = -20.0 , Ic_peak = -24.80000114
shot 1534: phi_e = -34.0 , Ic_peak = -8.0
shot 1528: phi_e = -160.0 , Ic_peak = -2.6000001
shot 1529: phi_e = -320.0 , Ic_peak = -5.4000001
```

This is consistent with the observation that decreasing the electron repeller potential (phi_e) decreases the signal amplitude. However, there is a small increase in signal amplitude from phi_e = -160V to phi_e = -320V. Again, these data points may be affected by secondary electron emission issues and may need to be removed from the analysis.

Determining the I-V curve

In [24]:
```
import numpy as np
```

The next cell establishes a dictionary called I_V_data, which organizes all of the Ic_peak data by their associated electron repeller potential (phi_e). The code initializes the dictionary then scans the shot_data dictionary. If the phi_e for a given shot is not already in I_V_data, it creates a new key for that phi_e value and pairs it with a numpy array, which contains the Ic_peak value. If the phi_e for a shot is already in the dictionary, it adds the Ic_peak value for the shot to the existing array.

In [43]:
```
I_V_data = {}

for shot_name in shot_data:
    phi_e   = shot_data[shot_name]['phi_e']
    Ic_peak = shot_data[shot_name]['Ic_peak']
    if phi_e not in I_V_data:
        I_V_data[phi_e] = np.array(Ic_peak)
    else:
        I_V_data[phi_e] = np.append(I_V_data[phi_e], Ic_peak)
```

The next step is to create numpy arrays of the electron repeller potentials, the energies associated with these potentials (E_min), and the mean and standard deviation of Ic_peak at each repeller potential. These arrays then need to be sorted by electron repeller potential because data is retrieved from dictionaries in arbitrary order. All of this is accomplished in the next cell.

In [44]:
```
phi_r        = np.empty(len(I_V_data))
Ic_peak_mean = np.empty(len(I_V_data))
Ic_peak_std  = np.empty(len(I_V_data))

Z = 1  # charge state; 1 for electrons

for i, phi_e in enumerate(I_V_data):
    phi_r[i]        = phi_e  # creates an array of the repeller pot
entials
    Ic_peak_mean[i] = I_V_data[phi_e].mean()
    Ic_peak_std[i]  = I_V_data[phi_e].std()

E = abs(Z*phi_r)  # creates an array of the minimum energies associ
ated with the repeller potentials

# the next lines sort the arrays in order of increasing repeller po
tential
sort_indices  = phi_r.argsort()
phi_r         = phi_r[sort_indices]
E             = E[sort_indices]
Ic_peak_mean  = Ic_peak_mean[sort_indices]
Ic_peak_std   = Ic_peak_std[sort_indices]
```

NOTE: the abs( ) used in the cell above is specific to electron analysis. This is not necessary when analyzing ion data.

In [47]:
```
# this plots the mean Ic_peak versus repeller potential with the ap
propriate error
sys_error = 0.0  # the systematic error of the Mochi.GEA is current
ly unknown
plt.errorbar(phi_r, Ic_peak_mean, yerr = Ic_peak_std + sys_error)

plt.xlabel('electron repeller potential [V]'), plt.ylabel('max coll
ector current [arbitrary units]')
plt.savefig('I-V_curve.png', dpi = 400)
plt.show()
```

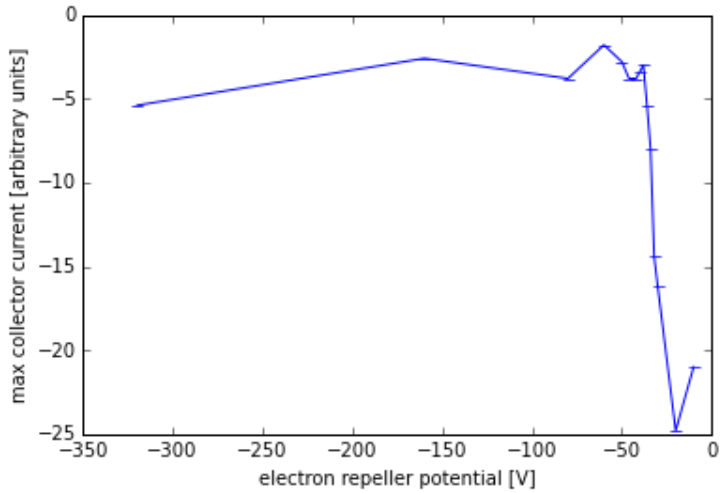

Note that the standard deviation (error) is zero in this case because only one data point was taken at each repeller potential.

The max collector current has arbitrary units because the raw data is a potential trace in volts, which must be converted to a current using some impedance. This impedance is frequency-dependent, so it must be measured or estimated and then convolved with the raw data. But this turns out to only scale the amplitude of the resulting energy distribution, and the amplitude is far less important than the shape and location. For this reason, the units are reported as arbitrary and this process is avoided.

Determining the electron energy distribution

The final step is to calculate the electron energy distribtution, g(E), from the I-V data. The distribution is equal to -dIc_peak/dE divided by the square root of E, with arbitrary units.

In [48]:
```
dE           = -1*np.gradient(E)
dIc_peak_mean = np.gradient(Ic_peak_mean, dE, edge_order=2)  # this
calculates dIc_peak_mean/dE

g_of_E = -dIc_peak_mean/np.sqrt(E)  # the electron energy distribut
ion g(E)
```

NOTE: the factor of -1 applied to dE is specific to electron analysis and must be removed when analyzing ion data. The energy distribution is equal to the negative of the derivative. But for electron analysis the absolute value of the repeller potential is taken to make the values of the energy array positive (positive kinetic energies). This reverses the sign of dE artificially.

In [49]:
```
plt.plot(E, g_of_E)
plt.axhline(color='black')
plt.xlabel('energy [eV]'), plt.ylabel('g(E) [arbitrary units]')
plt.savefig('energy_distribution.png', dpi = 400)
plt.show()
```

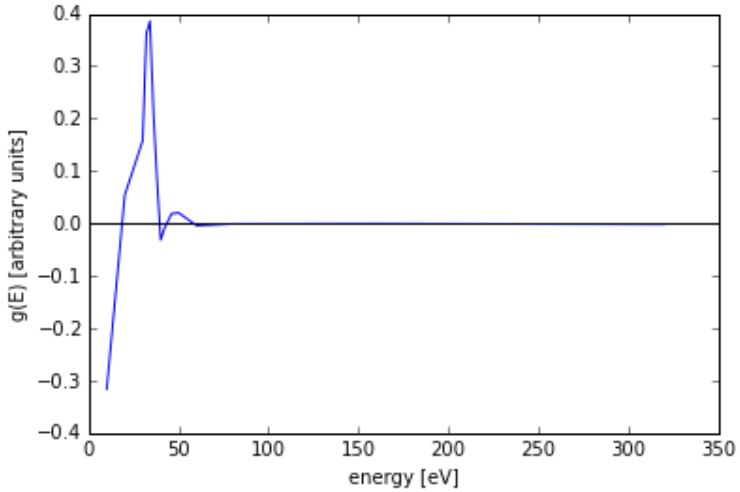

This looks somewhat like a Maxwellian centered at about 40eV. However, the value of g(E) is negative in a few locations, which is impossible because g(E) is defined as the number of particles per unit energy per unit volume. The derivative dI/dE is negative at these locations. This could be caused by an effect like secondary electron emission, where the collected current begins to rise again with increased repeller amplitude; or by shot-to-shot variability. Only one data point is taken at each repeller potential in this analysis. The derivative at these repeller potentials may actually be positive when averaged over many shots.

Estimating the electron temperature

An estimate of the electron temperature can be achieved by fitting a Maxwellian to g(E). The Maxwellian distribution of particle energies is proportional to sqrt(E)exp(-E/kT), where kT is the temperature and defines the spread of the distribution. The scale factor is dropped here because calculated g(E) has arbitrary scale. This distribution can also be shifted to start at a non-zero location, sqrt(E - shift)exp(-(E - shift)/kT), that is be related to the plasma potential and collector bias potential (0V in this case).

In [51]:
```
from scipy.optimize import curve_fit
```

In [52]:
```
def E_maxwellian(E, kT, shift):
    maxwellian = np.empty_like(E)
    for i, E_val in enumerate(E):
        if E_val <= shift:
            maxwellian[i] = 0.0
        if E_val > shift:
            maxwellian[i] = np.sqrt(E[i] - shift) * np.exp(-(E[i] -
shift)/kT)
    return maxwellian
```

A Maxwellian energy distribution (defined above) can be fit to the data if appropriate guesses for the temperature and shift are provided.

In [53]:
```
guess_kT    = 5.
guess_shift = 22.

max_opt, max_cov = curve_fit(E_maxwellian, E, g_of_E, p0=(guess_kT,
guess_shift))
max_fit          = E_maxwellian(E, max_opt[0], max_opt[1])
```

In [54]:
```
plt.plot(E, g_of_E,  label='measured g(E)')
plt.plot(E, max_fit, label='fitted Maxwellian')
plt.axhline(color='black')
plt.xlabel('energy [eV]'), plt.ylabel('g(E) [arbitrary units]')
plt.legend(loc='best')
plt.savefig('energy_distribution_with_fit.png', dpi = 400)
plt.show()

print 'fit kT =', max_opt[0], 'eV, ', 'fit shift =', max_opt[1], 'e
V'
print 'variance-covariance matrix:'
print max_cov
```

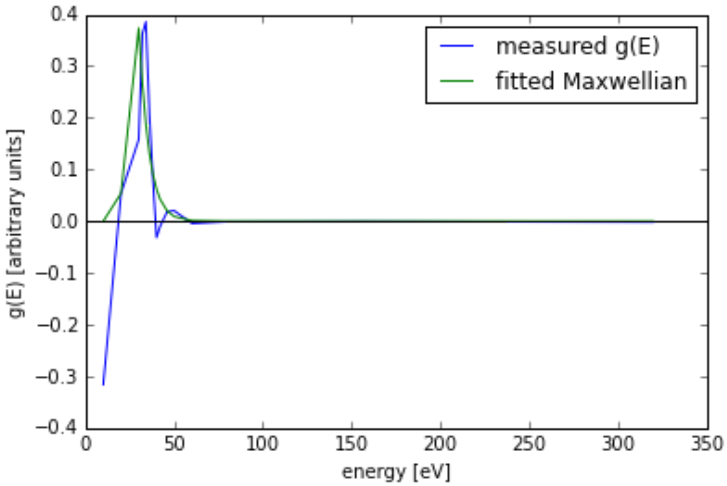


```
fit kT = 4.68443874795 eV,  fit shift = 19.9970926038 eV
variance-covariance matrix:
[[  1.91407203e-01  -5.75658881e-05]
 [ -5.75658881e-05   1.90732285e-04]]
```

The Maxwellian fits reasonably well and suggests that the electron temperature is about 5eV. A shift of 20eV suggests that the electrons enter the device with a potential about 20V below that of the collector bias potential (0V in this case). This could serve as an estimate of the plasma potential at this location. The diagonals of the variance-covariance matrix are the variances of the fit kT and fit shift parameters. The off-diagonal elements are the covariance between the two parameters.

Repeated analysis with total collected charge

Since the electron energy distribution determined by the maximum current method above goes negative in some locations, the alternate method of using the total collected charge is attempted below. This requires integrating the signal, which may smooth out the effect of the spikes in the current traces of some signals, thus smoothing out the I-V curve and g(E).

Determining the collected charge

In [55]:
```
from scipy import integrate
```

The next cell integrates each signal and adds the resulting total collected charge to the shot data dictionary, under the ket 'q_collected'.

In [56]:
```
for shot_name in shot_data:
    time      = shot_data[shot_name]['signal'][0]
    amplitude = shot_data[shot_name]['signal'][1]
    integral  = integrate.cumtrapz(amplitude, time)
    shot_data[shot_name]['q_collected'] = integral[-1]
```

In [57]:
```
print 'shot 1525:', 'phi_e =', shot_data['shot_1525']['phi_e'], ',
q_collected =', shot_data['shot_1525']['q_collected']
print 'shot 1534:', 'phi_e =', shot_data['shot_1534']['phi_e'], ',
q_collected =', shot_data['shot_1534']['q_collected']
print 'shot 1528:', 'phi_e =', shot_data['shot_1528']['phi_e'], ',
q_collected =', shot_data['shot_1528']['q_collected']
print 'shot 1529:', 'phi_e =', shot_data['shot_1529']['phi_e'], ',
q_collected =', shot_data['shot_1529']['q_collected']
```

```
shot 1525: phi_e = -20.0 , q_collected = -0.00397491023764
shot 1534: phi_e = -34.0 , q_collected = -0.00128163006734
shot 1528: phi_e = -160.0 , q_collected = -6.41099912862e-05
shot 1529: phi_e = -320.0 , q_collected = 3.69099973777e-05
```

This is consistent with the observation that increasing the electron repeller potential (phi_e) decreases the signal amplitude, and thus the charge collected (q_collected). Shot 1525 has an average amplitude of about -20A for about 200us, so the integral should be about -0.004C. The actual result is -0.00397C, very close. Shots 1528 and 1529 have very little collected charge (about 10^-5C), as is to be expected with a high repeller potential. The integration seems correct.

Determining the I-V curve

In [58]:
```
I_V_data = {}  # this redefines the I_V_data dictionary to include
collected charge, instead of Ic_peak

for shot_name in shot_data:
    phi_e       = shot_data[shot_name]['phi_e']
    q_collected = shot_data[shot_name]['q_collected']
    if phi_e not in I_V_data:
        I_V_data[phi_e] = np.array(q_collected)
    else:
        I_V_data[phi_e] = np.append(I_V_data[phi_e], q_collected)
```

In [59]:
```
phi_r           = np.empty(len(I_V_data))
q_collected_mean = np.empty(len(I_V_data))
q_collected_std  = np.empty(len(I_V_data))

Z = 1  # charge state; 1 for electrons

for i, phi_e in enumerate(I_V_data):
    phi_r[i]           = phi_e
    q_collected_mean[i] = I_V_data[phi_e].mean()
    q_collected_std[i]  = I_V_data[phi_e].std()

E = abs(Z*phi_r)  # creates an array of the minimum energies associ
ated with the repeller potentials

# the next lines sort the arrays in order of increasing repeller po
tential
sort_indices     = phi_r.argsort()
phi_r            = phi_r[sort_indices]
E                = E[sort_indices]
q_collected_mean = q_collected_mean[sort_indices]
q_collected_std  = q_collected_std[sort_indices]
```

NOTE: the abs( ) used in the cell above is specific to electron analysis and is not necessary for ion analysis.

In [60]:
```
# this plots the mean q_collected versus repeller potential with th
e standard deviation of q_collected as the error
sys_error = 0.0
plt.errorbar(phi_r, q_collected_mean, yerr = q_collected_std + sy
s_error)

plt.title('I-V curve')
plt.xlabel('electron repeller potential [V]')
plt.ylabel('charge collected [arbitrary units]')
plt.show()
```

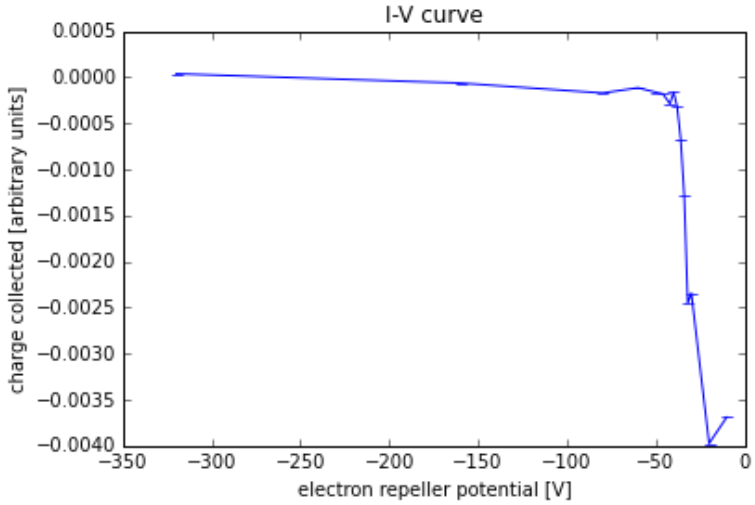

Determining the electron energy distribution

In [ ]:
```
dE                = -1*np.gradient(E)
dq_collected_mean = np.gradient(q_collected_mean, dE, edge_order=2)

g_of_E = -dq_collected_mean/np.sqrt(E)
```

NOTE: the factor of -1 applied to dE is specific to electron analysis and must be removed when analyzing ion data. The energy distribution is equal to the negative of the derivative. But for electron analysis the absolute value of the repeller potential is taken to make the values of the energy array positive (positive kinetic energies). This reverses the sign of dE artificially.

In [62]:
```
plt.plot(E, g_of_E)
plt.axhline(color='black')
plt.xlabel('energy [eV]'), plt.ylabel('g(E) [arbitrary units]')
plt.show()
```

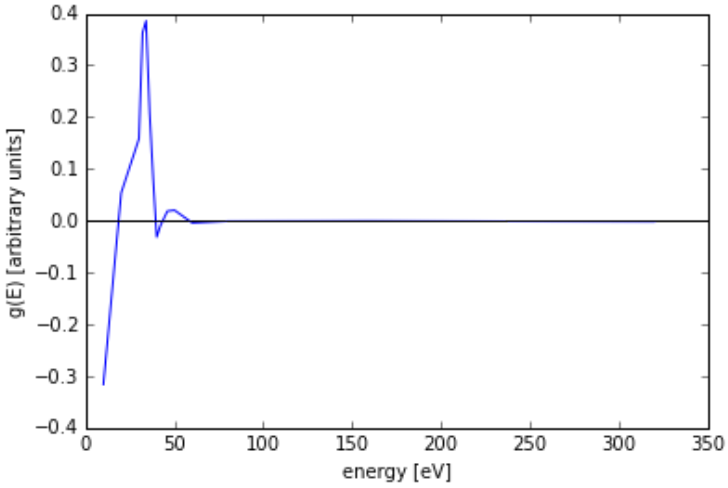

This did not remove all of the negative parts of the distribution, so the root cause is likely undersampling and shot-to-shot variability. The distribution looks similar to the distribution found using the peak current method.